Article

Analysis of Midrapidity p_T Distributions of Identified Charged Particles in Pb + Pb Collisions at $\sqrt{s_{nn}}$ = 5.02 TeV Using Tsallis Distribution with Embedded Transverse Flow

Khusniddin K. Olimov [1,2,*] , Fu-Hu Liu [3] , Anastasiya I. Fedosimova [4,5], Igor A. Lebedev [5] ,
Airton Deppman [6] , Kobil A. Musaev [1], Maratbek Z. Shodmonov [1] and Boburbek J. Tukhtaev [1]

[1] Physical-Technical Institute of Uzbekistan Academy of Sciences, Chingiz Aytmatov Str. 2b,
100084 Tashkent, Uzbekistan; qobilmusayev1986@gmail.com (K.A.M.);
maratbekshodmonov@yandex.ru (M.Z.S.); bobsash1416@gmail.com (B.J.T.)
[2] National University of Science and Technology MISIS (NUST MISIS), Almalyk Branch,
110105 Almalyk, Uzbekistan
[3] Institute of Theoretical Physics & Collaborative Innovation Center of Extreme Optics & State Key Laboratory
of Quantum Optics and Quantum Optics Devices, Shanxi University, Taiyuan 030006, China;
fuhuliu@sxu.edu.cn
[4] Institute of Nuclear Physics, Almaty 050032, Kazakhstan; ananastasia@list.ru
[5] Institute of Physics and Technology, Satbayev University, Almaty 050032, Kazakhstan;
lebedev692007@yandex.ru
[6] Instituto de Física, Universidade de São Paulo, São Paulo 05580-090, SP, Brazil; deppman@usp.br
* Correspondence: khkolimov@gmail.com

Abstract: The midrapidity transverse momentum distributions of the charged pions, kaons, protons,
and antiprotons, measured by ALICE Collaboration at ten centrality classes of Pb + Pb collisions at
$\sqrt{s_{nn}}$ = 5.02 TeV in the Large Hadron Collider (LHC, CERN, Switzerland), are successfully analyzed
using combined minimum χ^2 fits with a thermodynamically non-consistent, as well as thermody-
namically consistent, Tsallis function with transverse flow. The extracted non-extensivity parameter q
decreases systematically for all considered particle species with increasing Pb + Pb collision centrality,
suggesting an increase in the degree of system thermalization with an increase in collision centrality.
The results for q suggest quite a large degree of thermalization of quark–gluon plasma (QGP) created
in central Pb + Pb collisions at $\sqrt{s_{nn}}$ = 5.02 TeV with the average number of participant nucleons
$\langle N_{part} \rangle$ > 160. The obtained significantly different growth rates of transverse flow velocity, $\langle \beta_T \rangle$, in
regions $\langle N_{part} \rangle$ < 71 ± 7 and $\langle N_{part} \rangle$ > 71 ± 7 with the temperature parameter T_0 remaining constant
within uncertainties in region $\langle N_{part} \rangle$ > 71 ± 7 probably indicates that $\langle N_{part} \rangle \approx$ 71 ± 7 (corresponding
to $\langle dN_{ch}/d\eta \rangle \approx$ 251 ± 20) is a threshold border value for a crossover transition from a dense hadronic
state to the QGP phase (or mixed phase of QGP and hadrons) in Pb + Pb collisions at $\sqrt{s_{nn}}$ = 5.02 TeV.
The threshold border value for transverse flow velocity $\langle \beta_T \rangle \approx$ 0.46 ± 0.03 (corresponding to $\langle N_{part} \rangle$
$\approx$ 71 ± 7), estimated by us in Pb + Pb collisions at $\sqrt{s_{nn}}$ = 5.02 TeV, agrees well with the corresponding
border value $\langle \beta_T \rangle \approx$ 0.44 ± 0.02, recently obtained in Xe + Xe collisions at $\sqrt{s_{nn}}$ = 5.44 TeV, and
with almost constant $\langle \beta_T \rangle$ values extracted earlier in the Beam Energy Scan (BES) program of the
Relativistic Heavy-Ion Collider (RHIC, Brookhaven, GA, USA) in central Au + Au collisions in the
$\sqrt{s_{nn}}$ = 7.7 − 39 GeV energy range, where the threshold for QGP production is achieved. The correlations
between extracted T_0 and $\langle \beta_T \rangle$ parameters are found to be greatly different in regions $\langle \beta_T \rangle$ < 0.46
and $\langle \beta_T \rangle$ > 0.46, which further supports our result obtained for the threshold border value in Pb + Pb
collisions at $\sqrt{s_{nn}}$ = 5.02 TeV.

Keywords: heavy-ion collisions at the LHC; transverse momentum distributions of particles; non-
extensive Tsallis statistics with included transverse flow; thermalization of collision system; decon-
finement phase transition

1. Introduction

It is one of the main goals of modern experiments conducted using the RHIC (Relativistic Heavy-Ion Collider, Brookhaven, NY, USA) and LHC (Large Hadron Collider, CERN, Meyrin, Switzerland) to produce in collisions of high-energy heavy ions and investigate in detail quark–gluon plasma (QGP), the plasma state of almost-free quarks and gluons. Initially produced QGP expands hydrodynamically at an extremely high speed, reaching, one after the other, the chemical and kinetic freeze-out stages, respectively, which fixes the hadron abundances (yields) and final momenta of hadrons. Because of the extremely short lifespan of QGP, it is impossible to detect and measure its properties directly. Therefore, to extract important information on QGP and its evolution with changing collision energy and centrality, one has to analyze the yields, properties, and transverse momentum or/and (pseudo)rapidity spectra of the final particles with the help of efficient theoretical and phenomenological models. Pions, kaons, and (anti)protons account for the predominantly largest part of the final particles produced in high-energy collisions in the RHIC and LHC. Therefore, the production of these particles, consisting of light (u, d, and s) quarks, has been studied quite extensively [1–24] to deduce valuable information on the evolution and properties of produced hot and dense matter, and mechanisms of particle production at high-energy collisions.

The production and evolution of QGP are echoed in characteristic QGP signals, such as (multi)strangeness enhancement, jet quenching, development of strong collective flow, and J/ψ suppression, which have been detected and studied [25–35] in collisions of heavy ions at high energies in the RHIC and LHC. Based on the detection and thorough analysis of such signals, QGP has been discovered in collisions of heavy ions at high energies in the RHIC and LHC [21]. The obtained QGP matter presented fluid-like behavior with low viscosity [21]. The critical temperature, $T_c \approx 150$–170 MeV, and corresponding critical energy density, $\varepsilon_c \approx 1$ GeV/fm^3, for a phase transition from a nucleon to QGP matter have been obtained from lattice QCD (quantum chromodynamics) calculations [36,37]. The analogous QGP signatures with collective properties, similar to those in heavy-ion collisions, have also been observed in proton + proton collision events with high multiplicities [8–10,23,38–49] in the LHC.

It is necessary to briefly explain how the important parameters of the chemical and kinetic freeze-out stages are generally obtained. The particle abundancies (yields) are fitted with thermal or statistical hadronization models to extract the chemical freeze-out temperature (T_{ch}) and baryochemical potential (μ_b) [20,50–54]. The kinetic freeze-out temperature (T_0) and transverse expansion velocity (β_T) of particles at the moment of kinetic freeze-out are usually obtained from fitting the transverse momentum (p_T) distributions of particles with different theoretical and phenomenological models [1,20,23,24,49,55–67]: hydrodynamics-based blast-wave models, the blast-wave model with Boltzmann–Gibbs distribution (BGBW model), Tsallis (TBW model) statistics, and QCD-inspired Hagedorn (power law) function with embedded transverse. Such studies are extremely important for understanding the evolution of an early universe and structure of densely packed stars, as well as mechanisms of particle production at high energies [68–70].

Different modifications of the so-called Tsallis distribution function, based on non-extensive Tsallis statistics, have become efficient and standard functions for describing the transverse momentum distributions of particles in proton + proton collisions at high energies [71–83]. Compared to other power-law distributions, the Tsallis distribution function has a clear advantage expressed by its direct connection to thermodynamics through entropy [80]. In addition to the effective temperature parameter, the non-extensivity index q of the Tsallis function represents an important parameter, which shows the degree of deviation of particle transverse momentum distribution from the exponential Boltzmann–Gibbs distribution. Moreover, parameter q is said to measure the degree of non-equilibrium or that of the non-thermalization of a system [84]. The importance of the q parameter and its deep physical meaning, with a direct connection to thermodynamics, and the physical

significance of q in non-extensive statistical mechanics have been proven once again in the recent work [71] of Tsallis.

In Refs. [23,49,62–64,85], the transverse flow velocity was embedded using a simple Lorentz transformation into a QCD-inspired (power law) Hagedorn function to successfully reproduce the measured longer ranges of p_T spectra of the final particles in heavy-ion as well as proton + proton collisions at high energies. In a recent study [24], using the simple Lorentz transformation, we incorporated for the first time the transverse expansion velocity into both the simple, thermodynamically non-consistent, and thermodynamically consistent Tsallis functions to successfully analyze the centrality dependencies of p_T distributions of the charged pions, kaons, and (anti)protons in Xe + Xe collisions at $\sqrt{s_{nn}}$ = 5.44 TeV, measured by ALICE Collaboration in Ref. [12]. Compared to other hydrodynamics-based blast-wave models, the non-consistent Tsallis function with a transverse flow, as well as the thermodynamically consistent Tsallis function with a transverse flow, obtained for the first time in Ref. [24] and used in the present analysis, have fewer parameters, and each of them carries a physical meaning [24]. As indicated in Refs. [1,49,57,63,64], it is impossible to assign any physical meaning to collectivity parameters, such as transverse flow velocity and kinetic freeze-out temperature, obtained from separate model fits to p_T distribution of single-particle species. On the other hand, the simultaneous combined model fits to p_T distributions of all analyzed particle species in a given collision system can produce the physically meaningful collectivity parameters of the analyzed system [1,20,23,24,49,57,62–64,85]. The combined (global) model fits permit us to compare various collision systems using a few parameters [1,20,23,24,49,57,62–64,85].

The present study aims to investigate the midrapidity (mid-y) p_T distributions of identified charged particles, measured by the ALICE Collaboration [57] at different centralities of Pb + Pb collisions at $\sqrt{s_{nn}}$ = 5.02 TeV, applying combined model fits with both the non-consistent as well as thermodynamically consistent Tsallis functions with transverse flow, introduced and used for the first time in Ref. [24] to successfully study the collision centrality dependencies of mid-y p_T distributions of the identified charged particles in Xe + Xe collisions at $\sqrt{s_{nn}}$ = 5.44 TeV. The paper is organized as follows: the information about the experimental data and theoretical models is presented in Section 2; the analysis and results are presented in Section 3; and Section 4 summarizes the results and conclusions of the present analysis.

2. Experimental Data and Models

In the present study, we analyzed the experimental data obtained by ALICE Collaboration [57] at the LHC using the central barrel of the ALICE detector having full azimuthal coverage in the mid-(pseudo)rapidity $|\eta| < 0.8$ region [86]. In order to obtain transverse momentum distributions of the primary charged particles, the raw p_T distributions were corrected by ALICE Collaboration for misidentification probability, acceptance, reconstruction, and tracking efficiencies, and contaminations mostly due to weak decays of Λ and Σ^+ (affecting (anti)proton spectra), and of K_s^0 (affecting spectra of charged pions), and interactions with the material were computed and subtracted from the raw spectra. The p_T spectra were extracted for 0–5%, 5–10%, 10–20%, 20–30%, 30–40%, 40–50%, 50–60%, 60–70%, 70–80%, and 80–90% collision centralities [57]. The average values of the number of participant nucleons ($\langle N_{part} \rangle$) and charged-particle (pseudo-rapidity) multiplicity density ($\langle dN_{ch}/d\eta \rangle$) were obtained [57,87] by ALICE Collaboration using Glauber–Monte Carlo model calculations for the analyzed centrality groups of Pb + Pb collisions at $\sqrt{s_{nn}}$ = 5.02 TeV, which are presented in Table 1.

Table 1. The average number of participant nucleons and mean charged-particle multiplicity densities [57,87] in the analyzed groups of centralities of Pb + Pb collisions at $\sqrt{s_{nn}}$ = 5.02 TeV.

Centr.	$\langle N_{part} \rangle$	$\langle dN_{ch}/d\eta \rangle$
0–5%	383 ± 11	1943 ± 56
5–10%	331 ± 10	1587 ± 47
10–20%	262 ± 7	1180 ± 31
20–30%	188 ± 5	786 ± 20
30–40%	131 ± 4	512 ± 15
40–50%	87 ± 4	318 ± 12
50–60%	54 ± 3	183 ± 8
60–70%	31 ± 2	96 ± 6
70–80%	16 ± 2	45 ± 3
80–90%	7 ± 1	18 ± 2

There are various forms [62,75,76,80–83,88,89] of the Tsallis distribution function. They all demonstrate quite good quality fits of the experimental p_T spectra of particles originating from high-energy collisions. One of the simplest versions [82] of the Tsallis distribution is presented at mid-y (<y> = 0) by the following expression:

$$\frac{d^2N}{2\pi N_{ev} p_T dp_T dy} = C\left(1 + (q-1)\frac{m_T}{T}\right)^{-\frac{q}{q-1}}, \tag{1}$$

where C is the fitting constant, N_{ev} is the total number of inelastic collision events, $m_T = \sqrt{p_T^2 + m_0^2}$ is the transverse energy, m_0 is the rest mass of a hadron, T represents the effective temperature, and q is the so-called non-extensivity parameter. This function in Equation (1) is called the simple, thermodynamically non-consistent Tsallis distribution in the present study. Parameter q is important, and it shows the deviation of transverse momentum distributions from the exponential Boltzmann–Gibbs distribution. This parameter is also said to measure the non-equilibrium level [84]. At $q = 1$, the Tsallis distribution reduces to the exponential (equilibrated) Boltzmann–Gibbs distribution.

The following form [75,80–82] of the Tsallis function at mid-y (<y> = 0) obtained at zero chemical potential μ (μ approaches zero and is negligible at high-collision energies at the LHC) results in consistent thermodynamics for the pressure, temperature, particle number, energy, and entropy densities:

$$\frac{d^2N}{2\pi N_{ev} p_T dp_T dy} = C_q m_T\left(1 + (q-1)\frac{m_T}{T}\right)^{-q/(q-1)}, \tag{2}$$

which is referred to as a consistent Tsallis function or Tsallis function with thermodynamical consistence in the present analysis. The thermodynamical consistence of this function has been proven in Ref. [75]. Here, C_q is the fitting constant, which is related linearly to the system's volume (V) [75,80] through the expression $C_q = gV/(2\pi)^3$, where g is the degeneracy factor equal to 2, 3, 4 for protons, pions, and kaons, respectively.

The T values extracted from fits by Tsallis functions in Equations (1) and (2) denote the effective temperature, which contains the effects of both the thermal motion and collective flow (expansion). The transverse expansion velocity should be embedded into the Tsallis distribution function in order to disentangle these two effects.

In Refs. [23,49,62–64,85], the transverse flow was incorporated into a QCD-inspired Hagedorn function, $\frac{d^2N}{2\pi N_{ev} p_T dp_T dy} = C_n\left(1 + \frac{m_T}{p_0}\right)^{-n}$, by setting $p_0 = nT_0$ and applying the simple Lorentz transformation $m_T \rightarrow \langle\gamma_T\rangle\cdot(m_T - p_T\langle\beta_T\rangle)$ to create the final expression:

$$\frac{d^2N}{2\pi N_{ev} p_T dp_T dy} = C_n\left(1 + \langle\gamma_T\rangle\frac{(m_T - p_T\langle\beta_T\rangle)}{nT_0}\right)^{-n}, \tag{3}$$

where C_n is the fitting constant, $\langle\gamma_T\rangle = 1/\sqrt{1 - \langle\beta_T\rangle^2}$, $< \beta_T >$ is the average transverse flow velocity, T_0 is the parameter estimating the kinetic freeze-out temperature, and n is the free parameter. The function in Equation (3) is called the Hagedorn function with an (embedded) transverse flow. The important substitution, $m_T \rightarrow \langle\gamma_T\rangle\cdot(m_T - p_T\langle\beta_T\rangle)$, used to derive Equation (3) represents the Lorentz transformation into a system co-moving with the average (common) transverse flow velocity, $< \beta_T >$, of particles if such a flow of particles exists in the co-moving frame [62]. The Hagedorn function with transverse flow, presented in Equation (3), can describe quite well the p_T spectra of particles produced in proton + proton and heavy-ion collisions in the RHIC and LHC in Refs. [23,49,62–64,85], allowing for the clear physical interpretation of the extracted parameters.

In comparison to Refs. [23,49,62–64,85], where the transverse expansion velocity was incorporated into the Hagedorn function resulting in the final Equation (3), in the present study, we embedded the transverse flow velocity into both the simple Tsallis function (Equation (1)) and Tsallis function with thermodynamical consistence (Equation (2)), as was performed for the first time in Ref. [24]. To describe mid-y p_T distributions, $\frac{d^2N}{N_{ev}dp_Tdy}$, of the identified charged particles in different centrality classes of Pb + Pb collisions at $\sqrt{s_{nn}}$ = 5.02 TeV, we embedded the transverse expansion velocity into the simple Tsallis function in Equation (1) by replacing $m_T \rightarrow \langle\gamma_T\rangle\cdot(m_T - p_T\langle\beta_T\rangle)$ [24]:

$$\frac{d^2N}{N_{ev}dp_Tdy} = 2\pi C p_T \left(1 + \langle\gamma_T\rangle\frac{(q-1)(m_T - p_T\langle\beta_T\rangle)}{T_0}\right)^{-q/(q-1)}, \tag{4}$$

which is called the simple or non-consistent Tsallis function with a transverse flow in the present study. One can observe that Equations (3) and (4) have similar mathematical structures and are almost equivalent, with the only difference being in parameters n and q.

Similarly, we inserted the transverse flow into the Tsallis function with thermodynamical consistence in Equation (2) by performing the $m_T \rightarrow \langle\gamma_T\rangle\cdot(m_T - p_T\langle\beta_T\rangle)$ transformation to obtain [24]

$$\frac{d^2N}{N_{ev}dp_Tdy} = 2\pi C_q p_T \langle\gamma_T\rangle(m_T - p_T\langle\beta_T\rangle)\left(1 + \langle\gamma_T\rangle\frac{(q-1)(m_T - p_T\langle\beta_T\rangle)}{T_0}\right)^{-q/(q-1)}, \tag{5}$$

which is called a thermodynamically consistent Tsallis function with a transverse flow in the present study. It is necessary to note that the functions in Equations (4) and (5) were derived for the first time and used successfully in Ref. [24] to describe the mid-y p_T distributions of the identified charged particles in different centrality classes of Xe + Xe collisions at $\sqrt{s_{nn}}$ = 5.44 TeV.

In the present study, we conducted simultaneous (combined) fits by the model functions, presented in Equations (4) and (5), of transverse momentum distributions of the studied particle species in each of the ten centrality groups employing the nonlinear curve fitting of Origin 9.1 Graphing and Data Analysis Software. T_0 and $\langle\beta_T\rangle$ were kept as the common (shared) parameters for all studied particle species during the combined fitting procedures.

The experimental data points in the figures of the present study show the combined (added) statistical and systematic errors. The combined errors are determined predominantly by the systematic uncertainties, which are much greater than the statistical ones. More details on the calculation of the systematic errors in the measured p_T distributions can be found in Ref. [57]. The minimum χ^2 fitting procedures were made taking into account the combined statistical and systematic errors as the weights $(1/(\text{error})^2)$ for the data points. The region $p_T < 0.5$ GeV/c in pion p_T distributions, which has a significant contribution from decays of baryon resonances, was excluded from fitting procedures, similar to Refs. [1,23,24,49,57,63,64,85]. In the present study, we used the same p_T intervals for combined fits with the model functions in Equations (4) and (5) as in Ref. [24]: [0.5–5.0] GeV/c for $\pi^+ + \pi^-$, [0.2–5.0] GeV/c for $K^+ + K^-$, and [0.3–5.0] GeV/c for $p + \overline{p}$. By using the identical p_T intervals and model functions, and the same analyzed particle species as

those in Ref. [24], we could directly compare the results obtained in the present study for Pb + Pb collisions at $\sqrt{s_{nn}}$ = 5.02 TeV with those extracted recently in Ref. [24] for Xe + Xe collisions at $\sqrt{s_{nn}}$ = 5.44 TeV.

3. Analysis and Results

The results of combined minimum χ^2 fits using the thermodynamically consistent Tsallis function with a transverse flow (Equation (5)) of midrapidity transverse momentum distributions of the charged pions, kaons, protons, and antiprotons in ten groups of centrality of Pb + Pb collisions at $\sqrt{s_{nn}}$ = 5.02 TeV are presented in Table 2. The corresponding combined minimum χ^2 fit curves with a consistent Tsallis function with a transverse flow in four different centrality classes of Pb + Pb collisions are presented in Figure 1.

Table 2. The results of combined minimum χ^2 fits with thermodynamically consistent Tsallis function with transverse flow (Equation (5)) of p_T spectra of particles in Pb + Pb collisions at $\sqrt{s_{nn}}$ = 5.02 TeV. *n.d.f.* denotes the number of degrees of freedom.

Centrality	$q\ (\pi^+ + \pi^-)$	$q\ (K^+ + K^-)$	$q\ (p+\bar{p})$	T_0 (MeV)	$\langle \beta_T \rangle$	$\chi^2/n.d.f.$
0–5%	1.088 ± 0.002	1.086 ± 0.002	1.088 ± 0.002	80 ± 3	0.60 ± 0.01	296/98
5–10%	1.093 ± 0.002	1.088 ± 0.002	1.090 ± 0.002	79 ± 3	0.59 ± 0.01	301/98
10–20%	1.096 ± 0.002	1.093 ± 0.002	1.092 ± 0.002	79 ± 3	0.58 ± 0.01	270/98
20–30%	1.102 ± 0.002	1.098 ± 0.002	1.095 ± 0.002	77 ± 2	0.57 ± 0.01	216/98
30–40%	1.108 ± 0.002	1.106 ± 0.002	1.098 ± 0.002	77 ± 2	0.53 ± 0.01	167/98
40–50%	1.117 ± 0.002	1.114 ± 0.002	1.100 ± 0.001	76 ± 2	0.49 ± 0.01	116/98
50–60%	1.124 ± 0.001	1.121 ± 0.001	1.107 ± 0.001	78 ± 2	0.43 ± 0.01	72/98
60–70%	1.131 ± 0.001	1.131 ± 0.001	1.112 ± 0.001	82 ± 2	0.33 ± 0.01	31/98
70–80%	1.136 ± 0.001	1.139 ± 0.001	1.116 ± 0.001	87 ± 2	0.22 ± 0.01	20/98
80–90%	1.142 ± 0.001	1.146 ± 0.001	1.118 ± 0.001	86 ± 3	0.14 ± 0.02	21/98

Table 3 presents the parameters obtained from combined minimum χ^2 fits using the thermodynamically non-consistent Tsallis function with a transverse flow (Equation (4)) of mid-y p_T distributions of the studied particle species in ten groups of centrality of Pb + Pb collisions at $\sqrt{s_{nn}}$ = 5.02 TeV. The corresponding combined minimum χ^2 fit curves by the non-consistent Tsallis function with transverse flow in four different centrality classes of Pb + Pb collisions are illustrated in Figure 2.

Table 3. The results of combined minimum χ^2 fits with thermodynamically non-consistent Tsallis function with transverse flow (Equation (4)) of p_T spectra of particles in Pb + Pb collisions at $\sqrt{s_{nn}}$ = 5.02 TeV.

| Centrality	$q\ (\pi^+ + \pi^-)$	$q\ (K^+ + K^-)$	$q\ (p+\bar{p})$	T_0 (MeV)	$\langle \beta_T \rangle$	$\chi^2/n.d.f.$
0–5%	1.083 ± 0.003	1.079 ± 0.004	1.085 ± 0.003	119 ± 4	0.59 ± 0.01	268/98
5–10%	1.089 ± 0.003	1.082 ± 0.004	1.087 ± 0.003	117 ± 4	0.59 ± 0.01	271/98
10–20%	1.093 ± 0.003	1.088 ± 0.003	1.090 ± 0.003	118 ± 4	0.58 ± 0.01	243/98
20–30%	1.102 ± 0.003	1.095 ± 0.003	1.093 ± 0.002	117 ± 4	0.56 ± 0.01	193/98
30–40%	1.110 ± 0.003	1.106 ± 0.003	1.097 ± 0.002	117 ± 3	0.53 ± 0.01	150/98
40–50%	1.122 ± 0.002	1.117 ± 0.003	1.101 ± 0.002	117 ± 3	0.48 ± 0.01	102/98
50–60%	1.132 ± 0.002	1.128 ± 0.002	1.109 ± 0.002	120 ± 3	0.41 ± 0.01	62/98
60–70%	1.141 ± 0.002	1.142 ± 0.002	1.115 ± 0.001	129 ± 3	0.32 ± 0.01	15/98
70–80%	1.148 ± 0.002	1.153 ± 0.002	1.120 ± 0.001	138 ± 3	0.20 ± 0.01	15/98
80–90%	1.157 ± 0.002	1.164 ± 0.002	1.123 ± 0.002	137 ± 5	0.12 ± 0.02	18/98
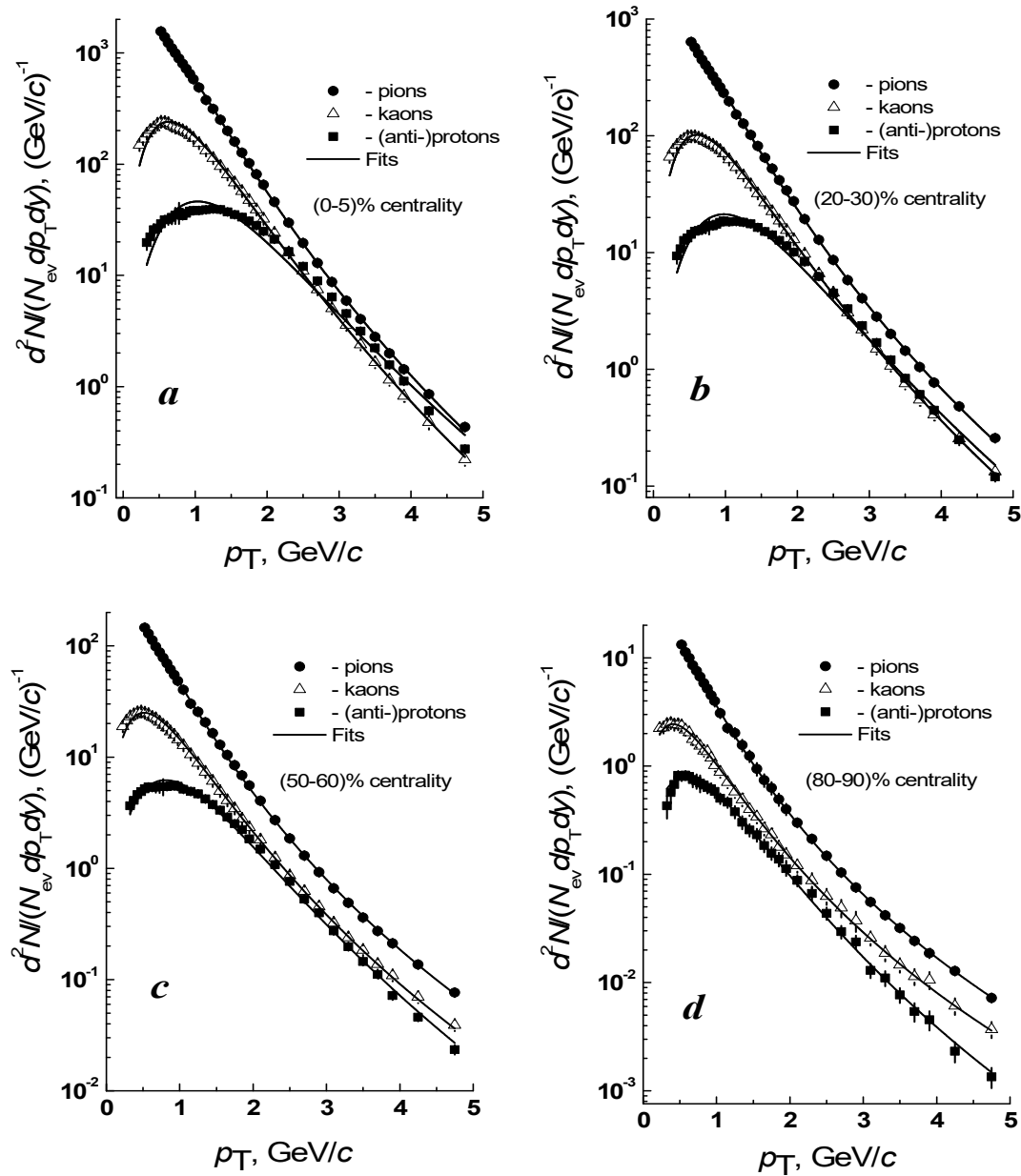
Figure 1. The obtained fit curves by consistent Tsallis function with transverse flow (Equation (5)) of the experimental midrapidity transverse momentum spectra of the charged pions (●), kaons (△), and protons and antiprotons (■) in Pb + Pb collisions at $\sqrt{s_{nn}}$ = 5.02 TeV at various centralities: 0–5% (**a**), 20–30% (**b**), 50–60% (**c**), and 80–90% (**d**).

Figures 1 and 2 and $\chi^2/n.d.f.$ values in Tables 2 and 3 show that the combined fits with both consistent and non-consistent Tsallis functions with transverse flows reproduce quite well the midrapidity transverse momentum distributions of the studied particle species in ten centrality classes of Pb + Pb collisions at $\sqrt{s_{nn}}$ = 5.02 TeV. It can be observed in Tables 2 and 3 that the fits by the simple non-consistent Tsallis function with a transverse flow result in slightly lower values of $\chi^2/n.d.f.$ than those by the consistent Tsallis function with transverse flow. Though the quality of the fits by the function in Equation (4) proved to be slightly better than those by the function in Equation (5) from the mathematical point of view, from a physics perspective it is still advantageous to use the function in Equation (5), based on the Tsallis distribution with thermodynamical consistence. This is because the consistent Tsallis distribution satisfies all the thermodynamic relations [75,80,81] (those for the pressure, temperature, entropy, and particle densities, etc.) resulting from the equations

of the first and second laws of thermodynamics. The clear advantage is, therefore, that temperature parameter T in the Tsallis distribution with thermodynamical consistence [75] can be considered as true temperature in the thermodynamic sense.
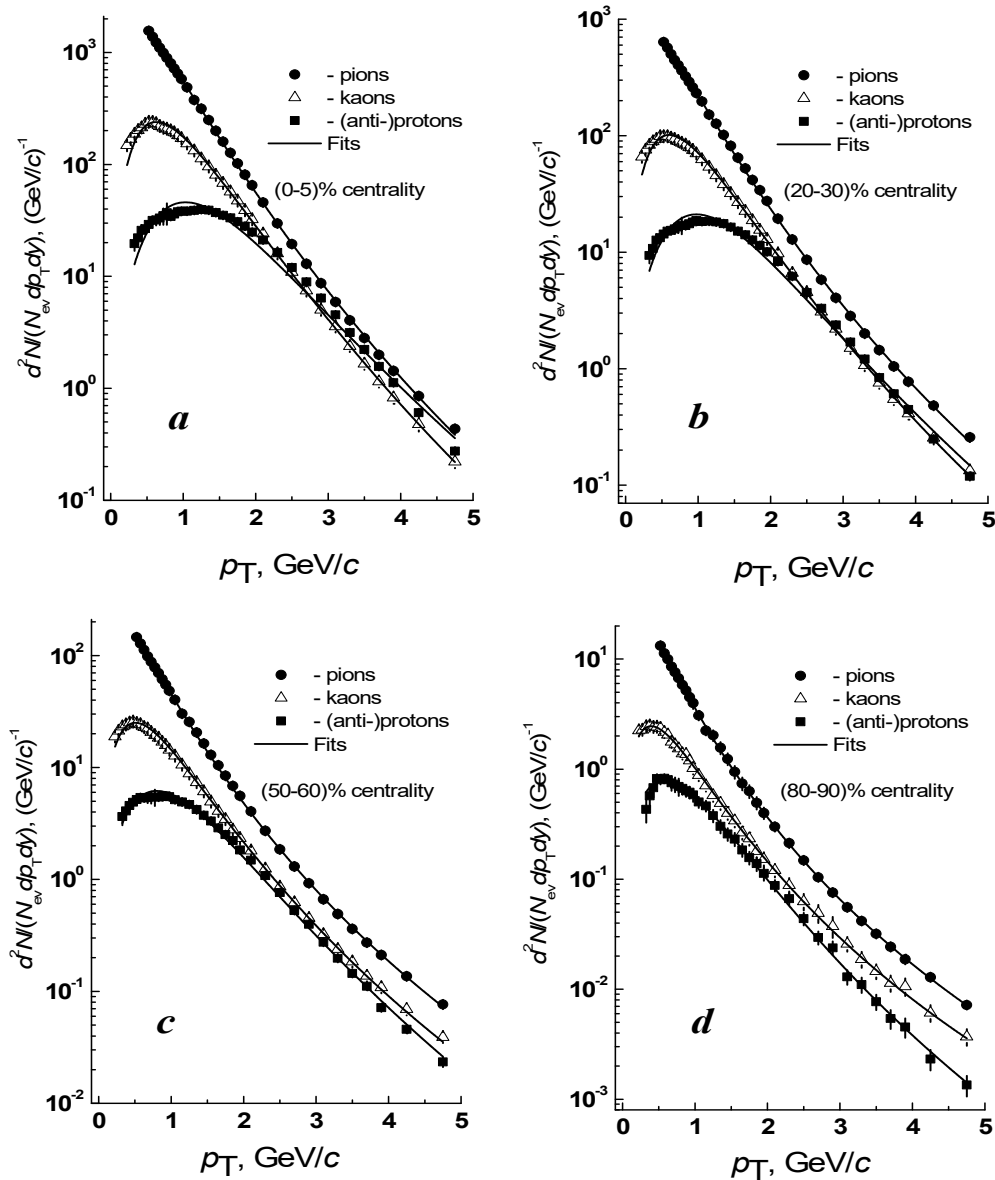

Figure 2. The obtained fit curves by non-consistent (simple) Tsallis function with transverse flow (Equation (4)) of the experimental midrapidity transverse momentum spectra of the charged pions (•), kaons (∆), and protons and antiprotons (■) in Pb + Pb collisions at $\sqrt{s_{nn}}$ = 5.02 TeV at various centralities: 0–5% (**a**), 20–30% (**b**), 50–60% (**c**), and 80–90% (**d**).

Figure 3 illustrates the corresponding $\langle N_{part} \rangle$ dependencies of the obtained parameters T_0, $\langle \beta_T \rangle$, and q of both consistent and non-consistent Tsallis functions with transverse flow for the studied particles in Pb + Pb collisions at $\sqrt{s_{nn}}$ = 5.02 TeV, extracted from combined fits and presented in Tables 2 and 3. In addition, the obtained $\langle \beta_T \rangle$ versus $\langle dN_{ch}/d\eta \rangle$ dependence is also presented. The analysis of $\langle \beta_T \rangle$ and T_0 behaviors and their dependencies on collision centrality and multiplicity of particles is important [23,24,49,66] because these parameters are also related to mapping the QCD phase diagram; however, the chemical freeze-out temperature is commonly used in such phase diagrams.
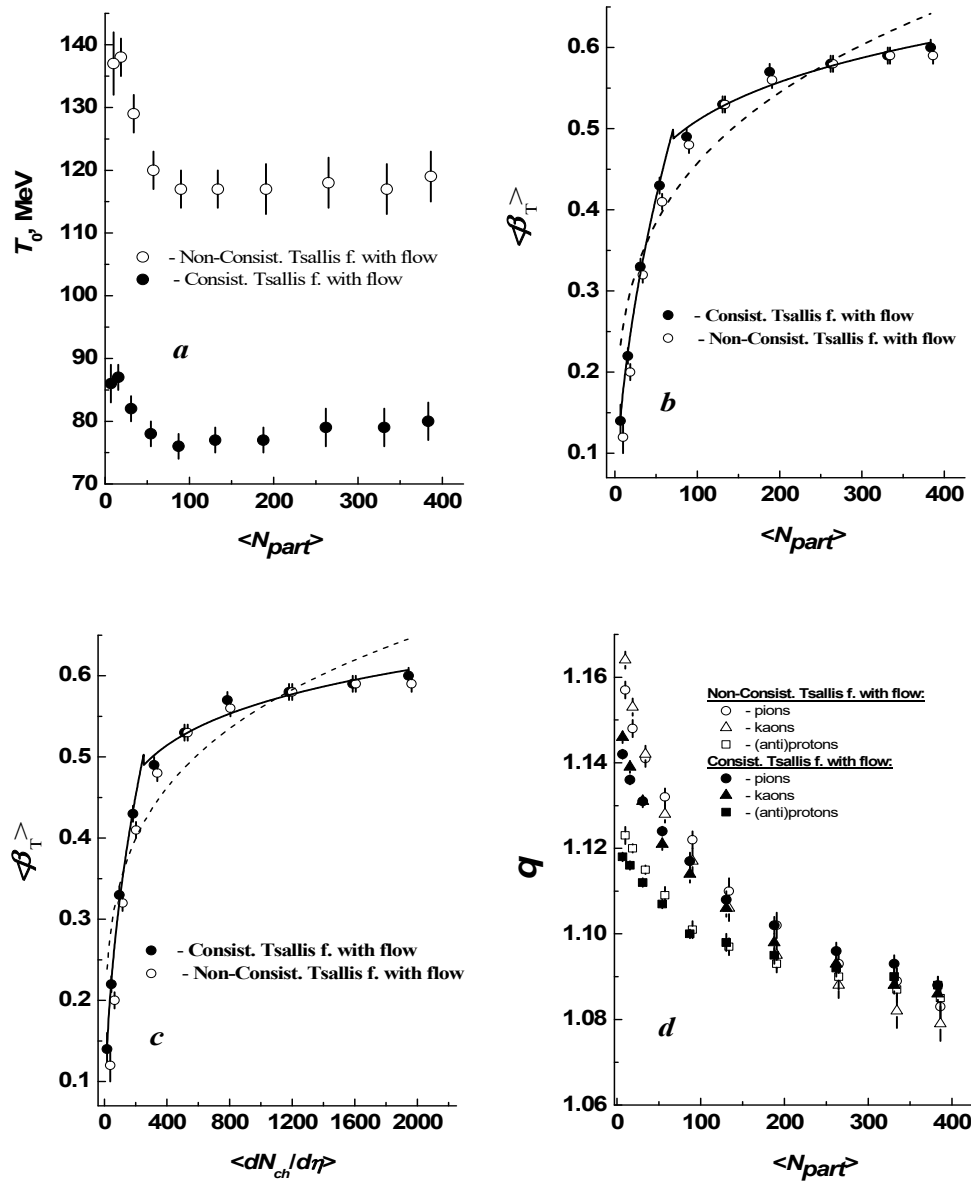
Figure 3. The $\langle N_{part} \rangle$ dependencies of the obtained T_0 (**a**) and $\langle \beta_T \rangle$ (**b**) parameters (●) of consistent Tsallis function with transverse flow (Equation (5)), presented in Table 2, in Pb + Pb collisions at $\sqrt{s_{nn}}$ = 5.02 TeV; (**c**) the $\langle \beta_T \rangle$ versus $\langle dN_{ch}/d\eta \rangle$ dependence; (**d**) the $\langle N_{part} \rangle$ dependence for the extracted q values of consistent Tsallis function with transverse flow (Equation (5)), presented in Table 2, for the charged pions (●), kaons (▲), and protons and antiprotons (■). The results (Table 3) obtained for the respective particles in Pb + Pb collisions at $\sqrt{s_{nn}}$ = 5.02 TeV using non-consistent Tsallis function with transverse flow (Equation (4)) are plotted by the corresponding open symbols. The dashed and solid curves in panels (**b**,**c**) are minimum χ^2 fits by the simple (single)-power (Equations (6) and (8)) and two-power (Equations (7) and (9)) functions, respectively, of the $\langle \beta_T \rangle$ versus $\langle N_{part} \rangle$ and $\langle \beta_T \rangle$ versus $\langle dN_{ch}/d\eta \rangle$ dependencies, respectively, extracted using consistent Tsallis function with transverse flow. For better visibility, the data (open symbols), extracted using non-consistent Tsallis function with transverse flow (Equation (4)), are slightly shifted along the positive directions of $\langle N_{part} \rangle$ and $\langle dN_{ch}/d\eta \rangle$ axes.

Figure 3a,b demonstrate that parameter T_0 as well as $\langle \beta_T \rangle$, obtained using both consistent and non-consistent Tsallis functions with transverse flows, similarly depend on $\langle N_{part} \rangle$. Figure 3a shows that T_0 values obtained from combined fits by the consistent Tsallis function with a transverse flow (Equation (5)) are systematically smaller as compared

to those from fits by a non-consistent Tsallis function with transverse flow (Equation (4)). This can be explained by the extra $\langle \gamma_T \rangle \cdot (m_T - p_T \langle \beta_T \rangle)$ factor in Equation (5), which is absent in Equation (4).

As can be observed in Figure 3a,b, the $\langle N_{part} \rangle$ dependencies of parameters T_0 and $\langle \beta_T \rangle$ in non-central Pb + Pb collisions in region $\langle N_{part} \rangle < 71 \pm 7$ differ substantially from those in semi-central and central Pb + Pb collisions in region $\langle N_{part} \rangle > 71 \pm 7$. The border value $\langle N_{part} \rangle \approx 71 \pm 7$ is estimated as the middle between the 4th and 5th points on the $\langle N_{part} \rangle$ axis (corresponding to 50–60% and 40–50% centrality in Table 1) in Figure 3a,b. Figure 3a shows that parameter T_0 on the whole decreases significantly in region $\langle N_{part} \rangle < 71 \pm 7$, then T_0 becomes quite stable being constant within fit uncertainties in region $\langle N_{part} \rangle > 71 \pm 7$. As observed from Figure 3b, the parameter $\langle \beta_T \rangle$ demonstrates significantly different growth rates with increasing $\langle N_{part} \rangle$ in non-central Pb + Pb collisions in the $\langle N_{part} \rangle < 71 \pm 7$ range and semi-central and central Pb + Pb collisions in region $\langle N_{part} \rangle > 71 \pm 7$. It is important to mention that the $\langle \beta_T \rangle$ values, obtained from combined model fits of longer p_T ranges (up to 5 GeV/c) at various centralities of Pb + Pb collisions at $\sqrt{s_{nn}}$ = 5.02 TeV in the present study and resented in Tables 2 and 3, proved to be compatible with the corresponding $\langle \beta_T \rangle$ at similar $\langle dN_{ch}/d\eta \rangle$ values in Pb + Pb collisions at $\sqrt{s_{nn}}$ = 2.76 TeV, obtained in Ref. [1] by ALICE Collaboration from combined Boltzmann–Gibbs blast-wave fits of p_T spectra of the studied particle species at lower p_T regions (up to 3 GeV/c). The absolute values of $\langle \beta_T \rangle$, obtained in the present study from combined fits of longer p_T intervals of particles by both thermodynamically consistent and thermodynamically non-consistent Tsallis functions with embedded transverse flow at ten centrality classes of Pb + Pb collisions at $\sqrt{s_{nn}}$ = 5.02 TeV, were found to be slightly lower than the $\langle \beta_T \rangle$ values extracted by ALICE Collaboration in Ref. [57] from combined Boltzmann–Gibbs blast-wave fits of the p_T spectra of particles at lower p_T ranges at the corresponding centralities of Pb + Pb collisions at $\sqrt{s_{nn}}$ = 5.02 TeV. The results of the present study for $\langle \beta_T \rangle$ versus collision centrality agree well with the known fact of increasing the transverse flow velocity with an increase in the centrality of heavy-ion collisions observed earlier in Refs. [1,20,24,34,57,60,63] and other works.

As observed from Figure 3b, the parameter $\langle \beta_T \rangle$ demonstrates a fairly high growth rate at $\langle N_{part} \rangle < 71 \pm 7$ and substantially lower rate of increase at $\langle N_{part} \rangle > 71 \pm 7$. To prove this observation, we fitted $\langle \beta_T \rangle$ versus $\langle N_{part} \rangle$ dependence in Figure 3b, obtained using the consistent Tsallis function with a transverse flow, with a single-power function

$$\langle \beta_T \rangle = A \cdot \langle N_{part} \rangle^{\alpha} \cdot (A\text{—fitting constant, } \alpha\text{—exponent parameter}) \tag{6}$$

as well as two-power functions:

$$\langle \beta_T \rangle = A_1 \cdot u\left(71 - \langle N_{part} \rangle\right) \cdot \langle N_{part} \rangle^{\alpha_1} + A_2 \cdot u\left(\langle N_{part} \rangle - 71\right) \cdot \langle N_{part} \rangle^{\alpha_2}, \tag{7}$$

where $u(t)$ is the Heaviside function ($u(t) = 0$ if $t < 0$, and $u(t) = 1$ if $t > 0$), A_1 and A_2 are fitting (normalization) constants, and α_1 and α_2 are exponent parameters.

As can be observed in Figure 3c, the parameter $\langle \beta_T \rangle$ demonstrates quite a high growth rate at $\langle dN_{ch}/d\eta \rangle < 251 \pm 20$ and a substantially smaller rate of increase at $\langle dN_{ch}/d\eta \rangle > 251 \pm 20$. The threshold border value $\langle dN_{ch}/d\eta \rangle \approx 251 \pm 20$, corresponding to border value $\langle N_{part} \rangle \approx 71 \pm 7$, was estimated as the middle point between $\langle dN_{ch}/d\eta \rangle$ values for 50–60% and 40–50% collision centralities in Table 1. Similarly to Figure 3b, we fitted the $\langle \beta_T \rangle$ versus $\langle dN_{ch}/d\eta \rangle$ dependence in Figure 3c, obtained using consistent the Tsallis function with transverse flow, with a single-power function

$$\langle \beta_T \rangle = A \cdot \langle dN_{ch}/d\eta \rangle^{\alpha} \cdot (A\text{—fitting constant, } \alpha\text{—exponent parameter}) \tag{8}$$

as well as a two-power function:

$$\beta_T = A_1 \cdot u(251 - \langle dN_{ch}/d\eta \rangle) \cdot \langle dN_{ch}/d\eta \rangle^{\alpha_1} + A_2 \cdot u(\langle dN_{ch}/d\eta \rangle - 251) \cdot \langle dN_{ch}/d\eta \rangle^{\alpha_2}. \tag{9}$$

Though, for the convenience, we used the same symbols for the parameters in Equations (6) and (8) (and in Equations (7) and (9)), they should be considered as different parameters in equations with different arguments of $\langle N_{part} \rangle$ and $\langle dN_{ch}/d\eta \rangle$.

The parameters obtained from minimum χ^2 fits of $\langle \beta_T \rangle$ versus $\langle N_{part} \rangle$ ($\langle \beta_T \rangle$ versus $\langle dN_{ch}/d\eta \rangle$) dependence in Figure 3b (Figure 3c) by the functions in Equations (6) and (7) (Equations (8) and (9)) are presented in Table 4 (Table 5). As can be observed in Figure 3b (Figure 3c) and $\chi^2/n.d.f.$ values in Table 4 (Table 5), the single-power function cannot satisfactorily describe the $\langle \beta_T \rangle$ versus $\langle N_{part} \rangle$ ($\langle \beta_T \rangle$ versus $\langle dN_{ch}/d\eta \rangle$) dependence. At the same time, the two-power function with two different exponent parameters in regions $\langle N_{part} \rangle < 71 \pm 7$ ($\langle dN_{ch}/d\eta \rangle < 251 \pm 20$) and $\langle N_{part} \rangle > 71 \pm 7$ ($\langle dN_{ch}/d\eta \rangle > 251 \pm 20$) reproduces these dependencies in Figure 3b,c very well. Significantly differing growth rates of $\langle \beta_T \rangle$ in regions $\langle N_{part} \rangle < 71 \pm 7$ ($\langle dN_{ch}/d\eta \rangle < 251 \pm 20$) and $\langle N_{part} \rangle > 71 \pm 7$ ($\langle dN_{ch}/d\eta \rangle > 251 \pm 20$) with T_0 staying constant within uncertainties in region $\langle N_{part} \rangle > 71 \pm 7$ ($\langle dN_{ch}/d\eta \rangle > 251 \pm 20$) possibly suggests that $\langle N_{part} \rangle \approx 71 \pm 7$ ($\langle dN_{ch}/d\eta \rangle \approx 251 \pm 20$) is a threshold border value for a crossover transition from a dense hadronic (nucleon) state to the QGP phase (or mixed phase of QGP and hadrons) in Pb + Pb collisions at $\sqrt{s_{nn}}$ = 5.02 TeV. We can estimate the average transverse flow velocity, $\langle \beta_T \rangle$, corresponding to a possible border value $\langle N_{part} \rangle \approx 71 \pm 7$ ($\langle dN_{ch}/d\eta \rangle \approx 251 \pm 20$) for a crossover transition to the QGP state (or mixed phase of QGP and hadrons) in Pb + Pb collisions. The threshold border value $\langle \beta_T \rangle \approx 0.46 \pm 0.03$, corresponding to $\langle N_{part} \rangle \approx 71 \pm 7$ ($\langle dN_{ch}/d\eta \rangle \approx 251 \pm 20$), was estimated as the middle between $\langle \beta_T \rangle$ values for 50–60% and 40–50% collision centralities in Table 2, obtained from combined fits with the function in Equation (5) of transverse momentum distributions of the considered particle species in Pb + Pb collisions at $\sqrt{s_{nn}}$ = 5.02 TeV.

Table 4. The results of minimum χ^2 fits with the functions in Equations (6) and (7) of $\langle \beta_T \rangle$ versus $\langle N_{part} \rangle$ dependence in Figure 3b, obtained using consistent Tsallis function with transverse flow (Equation (5)).

Fitting Function	Parameter Values	$\chi^2/n.d.f.$
Equation (6)	$A = 0.143 \pm 0.025$ $\alpha = 0.252 \pm 0.033$	159/8
Equation (7)	$A_1 = 0.052 \pm 0.007$ $\alpha_1 = 0.532 \pm 0.034$ $A_2 = 0.282 \pm 0.022$ $\alpha_2 = 0.129 \pm 0.014$	6/6

Table 5. The results of minimum χ^2 fits with the functions in Equations (8) and (9) of β_T versus $\langle dN_{ch}/d\eta \rangle$ dependence in Figure 3c, obtained using consistent Tsallis function with transverse flow (Equation (5)).

Fitting Function	Parameter Values	$\chi^2/n.d.f.$
Equation (8)	$A = 0.130 \pm 0.026$ $\alpha = 0.211 \pm 0.030$	177/8
Equation (9)	$A_1 = 0.038 \pm 0.006$ $\alpha_1 = 0.468 \pm 0.032$ $A_2 = 0.274 \pm 0.024$ $\alpha_2 = 0.105 \pm 0.012$	7/6

It is important to mention that similar results were obtained in our recent work [24] from the analysis of transverse momentum distributions of identified charged particles in different centrality classes of Xe + Xe collisions at $\sqrt{s_{nn}}$ = 5.44 TeV. The results, similar to those presented in Figure 3, but obtained in Ref. [24] for $\langle N_{part} \rangle$ dependencies of the extracted parameters T_0, $\langle \beta_T \rangle$, and q in Xe + Xe collisions at $\sqrt{s_{nn}}$ = 5.44 TeV, are demonstrated in Figure 4. The average transverse flow velocity, $\langle \beta_T \rangle$, presented quite a

large growth rate in region $\langle N_{part} \rangle < 44 \pm 5$ and a significantly smaller growth rate in range $\langle N_{part} \rangle > 44 \pm 5$ with increasing $\langle N_{part} \rangle$ in Xe + Xe collisions at $\sqrt{s_{nn}}$ = 5.44 TeV [24]. Interestingly, the probable crossover transition border to the QGP state (or mixed phase of QGP and hadrons) was estimated to be between 50–60% and 40–50% collision centralities coinciding for both Xe + Xe collisions at $\sqrt{s_{nn}}$ = 5.44 TeV in Ref. [24] and Pb + Pb collisions at $\sqrt{s_{nn}}$ = 5.02 TeV in the present analysis. The significantly different growth rates of $\langle \beta_T \rangle$ in regions $\langle N_{part} \rangle < 44 \pm 5$ and $\langle N_{part} \rangle > 44 \pm 5$ with parameter T_0 stabilizing and becoming practically constant in range $\langle N_{part} \rangle > 44 \pm 5$ were observed in Xe + Xe collisions [24], indicating that $\langle N_{part} \rangle \approx 44 \pm 5$ (corresponding to $\langle dN_{ch}/d\eta \rangle \approx 158 \pm 20$) could be a threshold border value for a crossover transition from a dense hadronic state to the QGP phase (or mixed phase of QGP and hadrons) in Xe + Xe collisions at $\sqrt{s_{nn}}$ = 5.44 TeV. It is interesting to note that the threshold border value $\langle \beta_T \rangle \approx 0.44 \pm 0.02$ (corresponding to $\langle N_{part} \rangle \approx 44 \pm 5$ and $\langle dN_{ch}/d\eta \rangle \approx 158 \pm 20$), recently estimated in Xe + Xe collisions at $\sqrt{s_{nn}}$ = 5.44 TeV in Ref. [24], agreed within uncertainties with the corresponding $\langle \beta_T \rangle \approx 0.46 \pm 0.03$ obtained for Pb + Pb collisions at $\sqrt{s_{nn}}$ = 5.02 TeV in the present analysis, and with nearly constant $\langle \beta_T \rangle$ values extracted from the BES program at the RHIC [20] in central Au + Au collisions in the $\sqrt{s_{nn}}$ = 7.7–39 GeV energy range, where the threshold for QGP production is surely reached [20,90–94].

It is worth presenting in more detail the results of Ref. [20], where the chemical and kinetic freeze-out temperatures and average transverse flow velocities extracted in central (0–5%) Au + Au collisions at BES energies from $\sqrt{s_{nn}}$ = 7.7 to 39 GeV are compared with those obtained in central (0–5% and 0–7% centrality) heavy-ion collisions at AGS, SPS, top RHIC, and up to LHC energies (see Figure 38 in Ref. [20]). The extracted $\langle \beta_T \rangle$ increased at low $\sqrt{s_{nn}} < 7.7$ GeV energies and remained nearly constant across BES energies in central Au + Au collisions, changing from 0.44 ± 0.04 at $\sqrt{s_{nn}}$ = 7.7 GeV to 0.49 ± 0.04 at $\sqrt{s_{nn}}$ = 39 GeV [20]. After it, $\langle \beta_T \rangle$ gradually and steadily increased to LHC energies [20]. The obtained chemical freeze-out temperature presented an increase from $\sqrt{s_{nn}}$ = 7.7 to 19.6 GeV, then remained constant within the errors across higher BES, top RHIC, and up to LHC energies [20]. The chemical freeze-out temperature proved to be $\approx 160 \pm 5$ MeV in central heavy-ion collisions in the $\sqrt{s_{nn}} \geq 19.6$ GeV range [20], agreeing with the critical deconfinement phase transition temperature, $T_c \approx 150$–170 MeV, coming from lattice QCD calculations [36,37]. The yield of pions is characterized by a linear increase with increasing $\sqrt{s_{nn}}$ at lower collision energies, and it shows a kink structure at $\sqrt{s_{nn}} \approx 19.6$ GeV in central Au + Au collisions at the BES [20]. This has been interpreted as a clear change in the mechanism of particle production at $\sqrt{s_{nn}} \approx 19.6$ GeV [20].

As observed in Figure 3d, the parameter of non-extensivity q for the charged pions, kaons, and (anti)protons, resulting from both consistent and non-consistent Tsallis functions with transverse flow, shows similar dependencies on $\langle N_{part} \rangle$. The q values demonstrate a systematic decrease with increasing $\langle N_{part} \rangle$ and collision centrality for all studied particle species. A similar result, as observed in Figure 4c, is obtained for q versus $\langle N_{part} \rangle$ dependencies for the analyzed particle species in Xe+Xe collisions at $\sqrt{s_{nn}}$ = 5.44 TeV in Ref. [24]. This observation is in agreement with the fact that the level of thermalization of the system increases with increasing centrality of heavy-ion collisions at high energies. The relation $q(\text{pions}) \approx q(\text{kaons}) > q(\text{anti(protons)})$ was satisfied, as observed in Figure 3c, which agrees with the $q(\text{mesons}) > q(\text{baryons})$ relation found previously in high-energy collisions in Refs. [23,49,63,82,83,85,95]. On the whole, the gap between $q(\text{mesons})$ and $q(\text{baryons})$ decreases with an increase in Pb + Pb collision centrality, as observed in Figure 3c, and $q(\text{mesons})$ practically coincides within uncertainties with $q(\text{baryons})$ in central collisions with $\langle N_{part} \rangle > 160$. This could indicate quite a large degree of thermalization of QGP produced in central Pb + Pb collisions at $\sqrt{s_{nn}}$ = 5.02 TeV with $\langle N_{part} \rangle > 160$.
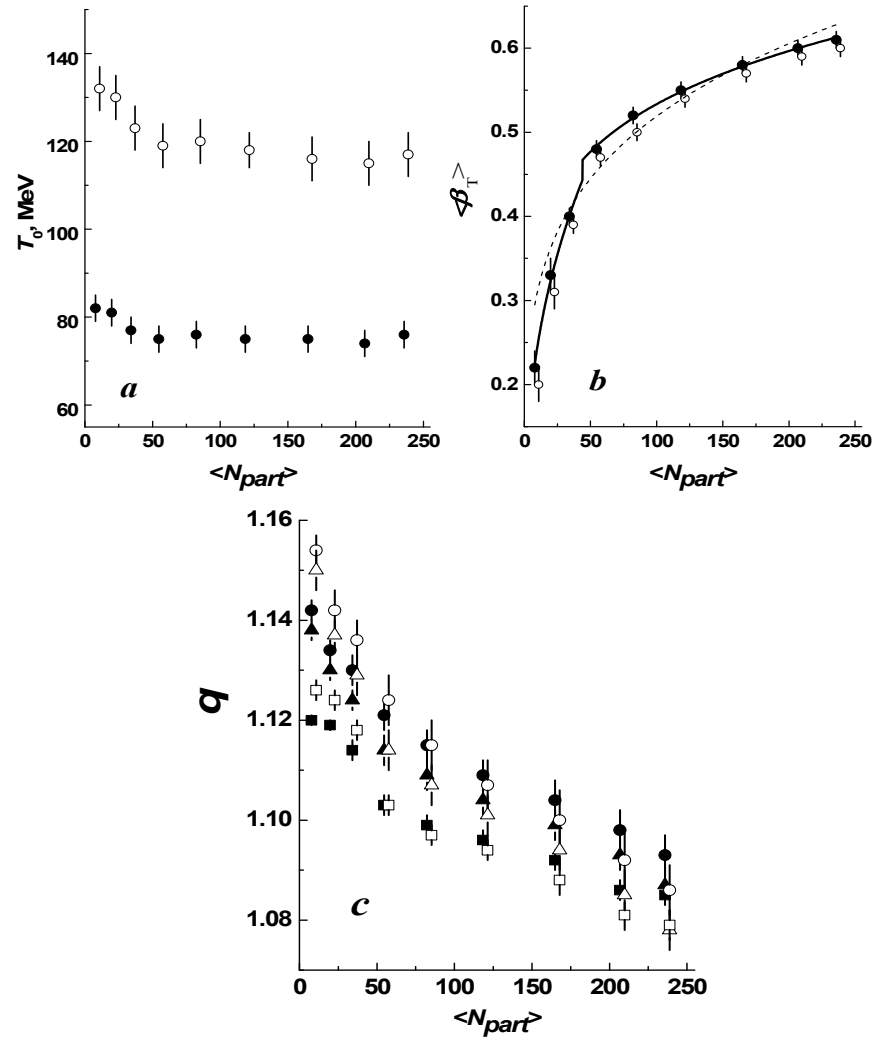
Figure 4. The same as Figure 3, but obtained in Ref. [24] for $\langle N_{part} \rangle$ dependencies of the extracted parameters T_0 (**a**), β_T (**b**), and q (**c**) in Xe+Xe collisions at $\sqrt{s_{nn}} = 5.44$ TeV. The dashed and solid curves in panel (**b**) are minimum χ^2 fits by the simple (single)-power and two-power functions, respectively, of the β_T versus $\langle N_{part} \rangle$ dependence, obtained using thermodynamically consistent Tsallis function with transverse flow (Equation (5)). For better visibility, the data (open symbols) extracted using thermodynamically non-consistent Tsallis function with transverse flow (Equation (4)) are shifted by +3 units along the positive direction of the $\langle N_{part} \rangle$ axis.

Quite a significant correlation exists [1,24] between the temperature and flow velocity parameters. To verify it quantitatively, we studied the correlations between the extracted parameters T_0 and $\langle \beta_T \rangle$, presented in Tables 2 and 3. The dependencies of T_0 versus $\langle \beta_T \rangle$ parameters extracted from fits with consistent (Equation (5)) and non-consistent (Equation (4)) Tsallis functions with transverse flow and presented in Tables 2 and 3 are illustrated in Figure 5a,b, respectively. The 1-sigma confidence ellipse of the covariance of the parameters T_0 and $\langle \beta_T \rangle$, corresponding to a 68% confidence interval, and the calculated Pearson correlation coefficient, r_{xy}, between parameters T_0 and $\langle \beta_T \rangle$ are also presented in the figures. It is necessary to mention that the Pearson correlation coefficient indicates the degree of a linear correlation between two sets of data (two parameter sets), and it can adopt values between -1 and $+1$. The orientations and shapes of the confidence ellipses and values of r_{xy} in Figure 5a,b show the high degree of anticorrelation (negative correlation) between parameters T_0 and $\langle \beta_T \rangle$ for fits by both consistent and non-consistent Tsallis functions with transverse flows. As can be observed in Figure 5a,b, the r_{xy} values

are close to −1 in both cases, and they also indicate a noticeably greater degree of negative correlation between parameters T_0 and $\langle \beta_T \rangle$ in Table 3 than that in Table 2.
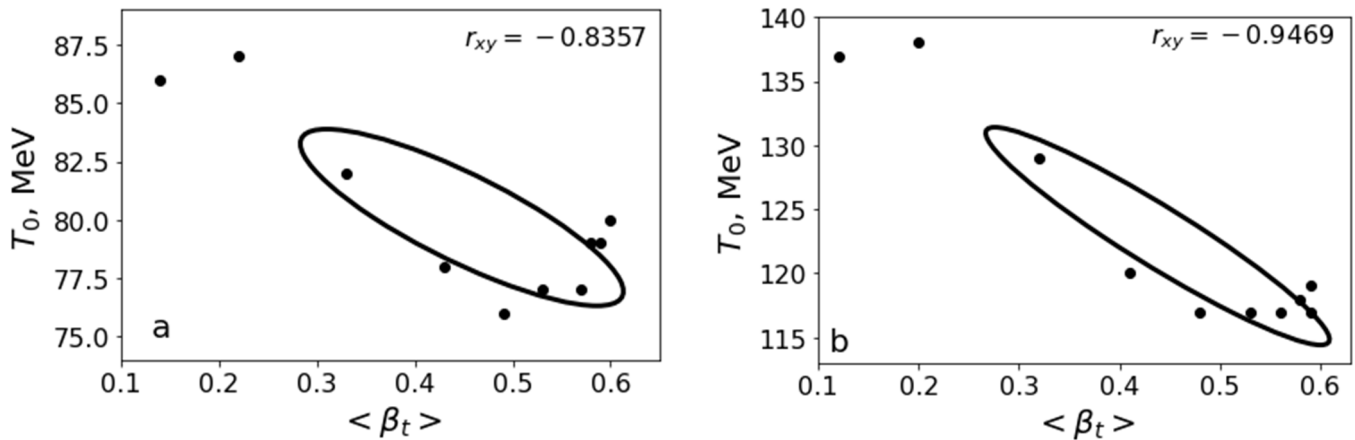

Figure 5. (a)—Dependence of T_0 versus $\langle \beta_T \rangle$ parameters (●) obtained from fits with consistent Tsallis functions with transverse flow (Equation (5)) and presented in Table 2. **(b)**—Dependence of T_0 versus $\langle \beta_T \rangle$ parameters (●) obtained from fits with non-consistent Tsallis functions with transverse flows (Equation (4)) and presented in Table 3. The 1-sigma confidence ellipse (corresponding to a 68% confidence interval) of the covariance of parameters T_0 and $\langle \beta_T \rangle$ and the calculated Pearson correlation coefficient, r_{xy}, between T_0 and $\langle \beta_T \rangle$ are also shown in the figures.

We presented above that the extracted parameter $\langle \beta_T \rangle$ demonstrates significantly differing growth rates in regions $\langle N_{part} \rangle < 71 \pm 7$ and $\langle N_{part} \rangle > 71 \pm 7$, and T_0 remains practically constant in region $\langle N_{part} \rangle > 71 \pm 7$, which probably indicates that $\langle N_{part} \rangle \approx 71 \pm 7$ ($\langle dN_{ch}/d\eta \rangle \approx 251 \pm 20$) is a border value for a crossover transition from a dense hadronic state to the QGP phase (or mixed phase of QGP and hadrons) in Pb + Pb collisions at $\sqrt{s_{nn}}$ = 5.02 TeV. The border value $\langle \beta_T \rangle \approx 0.46 \pm 0.03$, corresponding to $\langle N_{part} \rangle \approx 71 \pm 7$, was estimated above from the $\langle \beta_T \rangle$ data presented in Table 2. As can be observed in Figure 5a, the characters of T_0 versus $\langle \beta_T \rangle$ dependence are remarkably different in regions $\langle N_{part} \rangle < 71 \pm 7$ and $\langle N_{part} \rangle > 71 \pm 7$. The analogous situation can be observed in Figure 5b. To check and quantify this observation, we studied the correlations between parameters T_0 and $\langle \beta_T \rangle$, presented in Figure 5a,b, separately in regions $\langle \beta_T \rangle < 0.46$ and $\langle \beta_T \rangle > 0.46$. The results of the separate analysis of the data presented in Figure 5a,b (Tables 2 and 3) in region $\langle \beta_T \rangle < 0.46$ are shown in Figure 6a,c, respectively. The corresponding results for the correlation analysis of the same data in region $\langle \beta_T \rangle > 0.46$ are demonstrated in Figure 6b,d, respectively. As can be observed in Figure 6a,c, the negative correlation between T_0 and $\langle \beta_T \rangle$ is quite strong in region $\langle \beta_T \rangle < 0.46$. In contrast to the strong negative correlation in region $\langle \beta_T \rangle < 0.46$, the correlation between parameters T_0 and $\langle \beta_T \rangle$ is significantly positive in region $\langle \beta_T \rangle > 0.46$ in Figure 6b,d. Hence, it can be observed that not only does parameter $\langle \beta_T \rangle$ show significantly differing growth rates in regions $\langle N_{part} \rangle < 71 \pm 7$ ($\langle \frac{dN_{ch}}{d\eta} \rangle < 251 \pm 20$) and $\langle N_{part} \rangle > 71 \pm 7$ ($\langle \frac{dN_{ch}}{d\eta} \rangle > 251 \pm 20$), but also the character of correlation between parameters T_0 and $\langle \beta_T \rangle$ differs considerably in the corresponding intervals $\langle \beta_T \rangle < 0.46$ and $\langle \beta_T \rangle > 0.46$. This further supports our conjecture that $\langle N_{part} \rangle \approx 71 \pm 7$ ($\langle dN_{ch}/d\eta \rangle \approx 251 \pm 20$) is probably a threshold border value for a crossover transition from a dense hadronic (nucleon) state to the QGP phase (or mixed phase of QGP and hadrons) in Pb + Pb collisions at $\sqrt{s_{nn}}$ = 5.02 TeV.
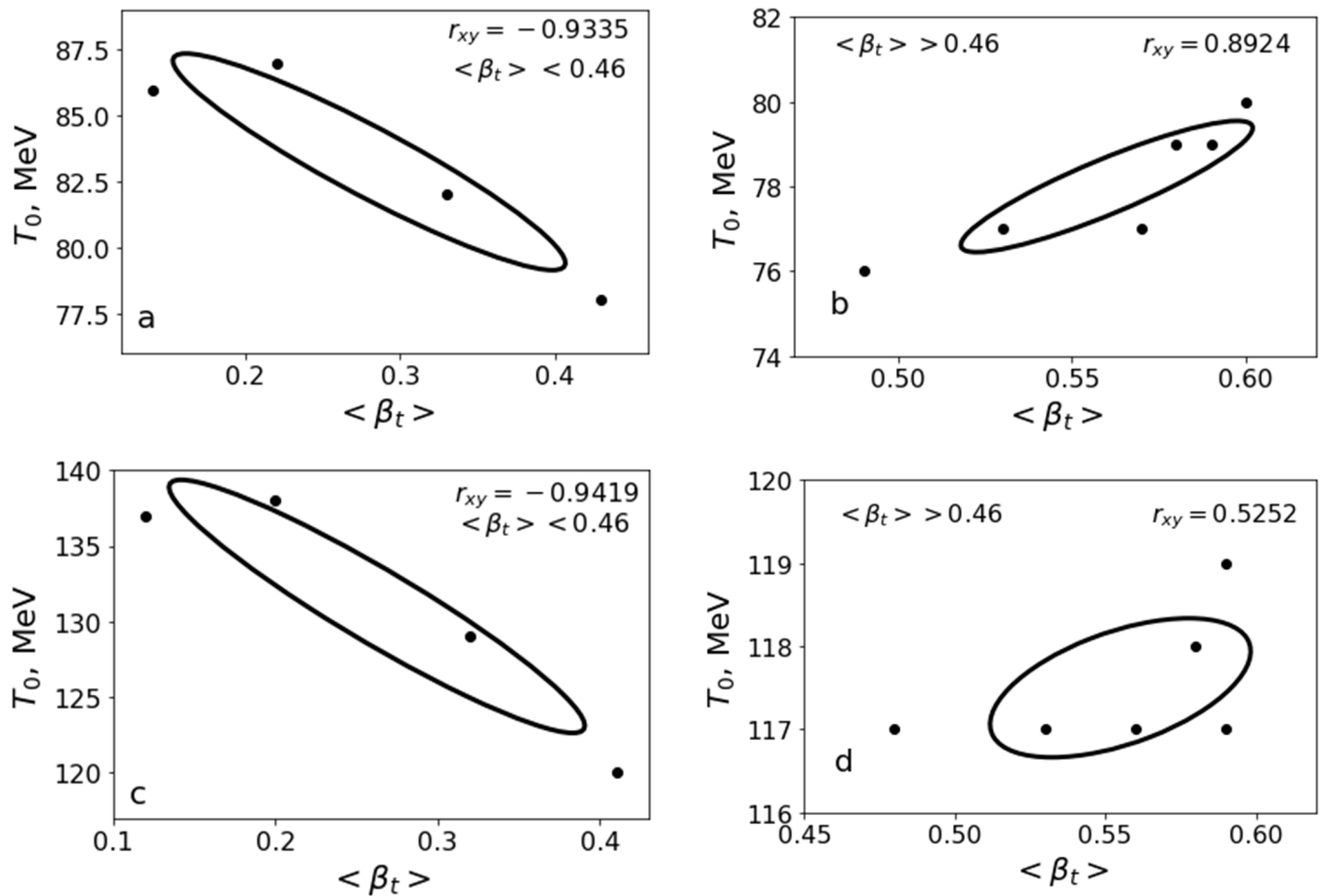
Figure 6. (**a**)—Dependence of T_0 versus $\langle \beta_T \rangle$ parameters (•) in region $\langle \beta_T \rangle < 0.46$ obtained from fits with thermodynamically consistent Tsallis functions with transverse flows (Equation (5)) and presented in Table 2. (**b**)—Dependence of T_0 versus $\langle \beta_T \rangle$ parameters (•) in region $\langle \beta_T \rangle > 0.46$ obtained from fits with thermodynamically consistent Tsallis functions with transverse flows (Equation (5)) and presented in Table 2. (**c**)—The same as in panel (**a**), but obtained from fits with non-consistent Tsallis functions with transverse flows (Equation (4)) and presented in Table 3. (**d**)—The same as in panel (**b**), but obtained from fits with non-consistent Tsallis functions with transverse flows (Equation (4)) and presented in Table 3. The 1-sigma confidence ellipse (corresponding to a 68% confidence interval) of the covariance of parameters T_0 and $\langle \beta_T \rangle$ and the calculated Pearson correlation coefficient, r_{xy}, between T_0 and $\langle \beta_T \rangle$ are also shown in the figures.

Now, we can directly compare the results for the threshold border values of $\langle N_{part} \rangle$, $\langle dN_{ch}/d\eta \rangle$, and $\langle \beta_T \rangle$ estimated in the present analysis in Pb + Pb collisions at $\sqrt{s_{nn}} = 5.02$ TeV, with those extracted in a recent study [24] for Xe + Xe collisions at $\sqrt{s_{nn}} = 5.44$ TeV, where the same theoretical model functions, methods, particle species, and identical p_T intervals were used. The results for the threshold border values of $\langle N_{part} \rangle$, $\langle dN_{ch}/d\eta \rangle$, and $\langle \beta_T \rangle$ estimated in Pb + Pb and Xe + Xe collisions [24] along with the ratios of the corresponding quantities for two collision types are presented in Table 6. As can be observed in Table 6, the ratio (1.61 ± 0.24) of the estimated border values of $\langle N_{part} \rangle$ in Pb + Pb and Xe + Xe collisions coincides with the ratio (1.59 ± 0.24) of the corresponding $\langle dN_{ch}/d\eta \rangle$ in these two collision types. It is interesting to compare these ratios for the border values of $\langle N_{part} \rangle$, as well as $\langle dN_{ch}/d\eta \rangle$, with the ratio of the mass numbers of the

corresponding ^{208}Pb and ^{132}Xe nuclei equal to $\frac{A(208_{\text{Pb}})}{A(132_{\text{Xe}})} \approx 1.58$. It can be observed that all the three ratios practically coincide with each other, satisfying the following relation:

$$\frac{\langle N_{part} \rangle_{\text{Pb + Pb}}}{\langle N_{part} \rangle_{\text{Xe + Xe}}} \approx \frac{\langle dN_{ch}/d\eta \rangle_{\text{Pb + Pb}}}{\langle dN_{ch}/d\eta \rangle_{\text{Xe + Xe}}} \approx \frac{A(208_{\text{Pb}})}{A(132_{\text{Xe}})} \approx 1.6 \tag{10}$$

Table 6. The threshold border values of $\langle N_{part} \rangle$, $\langle dN_{ch}/d\eta \rangle$, and $\langle \beta_T \rangle$ estimated in the present analysis for Pb + Pb collisions at $\sqrt{s_{nn}}$ = 5.02 TeV and compared to those extracted in a recent study [24] for Xe + Xe collisions at $\sqrt{s_{nn}}$ = 5.44 TeV. The ratios of the corresponding quantities for two collision types are presented in the last column.

Quantity	Xe + Xe Collisions at $\sqrt{s_{nn}}$ = 5.44 TeV [24]	Pb + Pb Collisions at $\sqrt{s_{nn}}$ = 5.02 TeV	$\frac{\text{Pb + Pb}}{\text{Xe + Xe}}$
$\langle N_{part} \rangle$	44 ± 5	71 ± 7	1.61 ± 0.24
$\langle dN_{ch}/d\eta \rangle$	158 ± 20	251 ± 20	1.59 ± 0.24
$\langle \beta_t \rangle$	0.44 ± 0.02	0.46 ± 0.03	1.07 ± 0.08

This result is quite interesting, and can be understood if one recalls that the volume of a nucleus is directly proportional to the number of nucleons, that is, to the mass number, A, of the nucleus. Similarly, the number of participant nucleons at some collision centrality is proportional to the volume of the overlap region of two identical colliding nuclei (such as in Pb + Pb and Xe + Xe collisions), which, in turn, should also be proportional to the volume of the nucleus, that is, to its mass number A.

In the end, it is interesting to mention the method of generic (non)extensive statistics (in which the underlying system autonomously manifests its extensive and non-extensive nature), which has been used to analyze the high-energy collision data at the LHC in Refs. [96–98] in comparison to the results of extensive Boltzmann and non-extensive Tsallis statistics. In Ref. [96], the yields and their ratios for the identified particles, measured by ALICE Collaboration, were described well using additive thermal approaches taking into account the missing resonance states, van der Waals repulsive interactions, finite volume corrections, and pion chemical potentials, as well as the light and strange quark occupation factors. In Ref. [97], the generic (non)extensive statistics approach was used to describe the transverse momentum spectra of strange hadrons in Pb + Pb collisions at $\sqrt{s_{nn}}$ = 2.76 TeV, p + Pb collisions at $\sqrt{s_{nn}}$ = 5.02 TeV, and in p + p collisions at $\sqrt{s_{nn}}$ = 7 TeV. The obtained results were compared to those extracted using non-extensive Tsallis and extensive Boltzmann statistics. The differences in the resulting fit parameters (temperature (T), volume (V), and non-extensive parameter d) among three types of statistics were observed in addition to the significant dependencies of the parameters on the size and type of the collision system [97]. It was determined that non-extensive parameter d decreases with increasing collision centrality and energy, indicating that the system departs from non-extensivity (non-equilibrium) and approaches extensivity (equilibrium) with the Boltzmann statistics becoming the proper statistical approach in describing the system in central collisions. It is important to mention that, in the present study, the non-extensivity parameter q values for all studied particle species, resulting from both consistent and non-consistent Tsallis functions with transverse flows, demonstrated a systematic decrease approaching $q \approx 1$ value with increasing collision centrality ($\langle N_{part} \rangle$). A similar result was obtained for q versus $\langle N_{part} \rangle$ dependencies for the analyzed particle species in Xe+Xe collisions at $\sqrt{s_{nn}}$ = 5.44 TeV in our recent study [24]. Considering that at $q \approx 1$ the non-extensive Tsallis distribution reduces to the exponential (equilibrated) Boltzmann–Gibbs distribution, our results for q versus $\langle N_{part} \rangle$ dependence agree well with those for the dependence of non-extensive parameter d on collision centrality in Ref. [97]. In Ref. [98], the extensive Boltzmann–Gibbs (BG) and non-extensive Tsallis statistics, generic (non)extensive statistics, and other empirical models were used for the description of the transverse momentum spectra of the charged pions, kaons, and protons produced in p + p and $A + A$

collisions in a wide interval of collision energies. The analytical expressions for the dependencies of the fit parameters on the energy, size of a collision system, and type of the used statistics were obtained [98]. It was deduced that the Tsallis distribution function is more effective within the lower p_T range compared to the higher p_T interval, and that the Tsallis statistics are more suited for p + p than $A + A$ collisions, while the Boltzmann statistics better describes $A+A$ collisions compared to p + p interactions [98]. It was concluded [98] that the generic (non)extensive statistics was well suited for describing the p_T spectra of the charged particles and their antiparticles in both p+p and $A+A$ collisions in a wide range of collision energies. As compared to the pure Tsallis statistics analysis (without embedded transverse flow) used for the comparison with other models in Ref. [98], for the description of p_T spectra of the identified particles at different centralities of Pb + Pb collisions at $\sqrt{s_{nn}}$ = 5.02 TeV in the present study, we used both thermodynamically non-consistent as well as thermodynamically consistent Tsallis distribution functions with incorporated transverse flows (presented in Equations (4) and (5)), which were derived and applied to successfully reproduce the transverse momentum spectra of identified particles in a range up to p_T = 5 GeV/c at various centralities of Xe + Xe collisions at $\sqrt{s_{nn}}$ = 5.44 TeV in our recent study [24]. As observed in Figures 1 and 2, both thermodynamically non-consistent as well as thermodynamically consistent Tsallis functions with embedded transverse flows could reproduce quite well the p_T spectra of the charged pions, kaons, and (anti)protons in the region up to p_T = 5 GeV/c at various centralities of Pb + Pb collisions at $\sqrt{s_{nn}}$ = 5.02 TeV in the present study.

4. Summary and Conclusions

　　We analyzed the mid-y p_T distributions of the charged pions, kaons, and protons and antiprotons measured by ALICE Collaboration at ten centrality classes of Pb + Pb collisions at $\sqrt{s_{nn}}$ = 5.02 TeV, applying combined minimum χ^2 fits with the non-consistent as well as thermodynamically consistent Tsallis functions with transverse flow. Combined fits of mid-y p_T distributions of $(\pi^+ + \pi^-)$, $(K^+ + K^-)$ and $(p + \overline{p})$ with both non-consistent and thermodynamically consistent Tsallis functions with transverse flows reproduced quite satisfactorily the spectra of analyzed particle species in all studied groups of Pb + Pb collision centrality.

　　Combined fits by both consistent and non-consistent Tsallis functions with transverse flow resulted in similar collision centrality ($\langle N_{part} \rangle$) dependencies of the parameters T_0, $\langle \beta_T \rangle$, and q, obtained in Pb + Pb collisions at $\sqrt{s_{nn}}$ = 5.02 TeV. The parameter $\langle \beta_T \rangle$ demonstrated a fairly large growth rate at $\langle N_{part} \rangle < 71 \pm 7$ and substantially lower rate of increase at $\langle N_{part} \rangle > 71 \pm 7$. This observation was verified quantitatively: the single-power function failed to describe $\langle \beta_T \rangle$ versus $\langle N_{part} \rangle$ dependence in the whole $\langle N_{part} \rangle$ range, whereas the two-power function with two different exponent parameters in regions $\langle N_{part} \rangle < 71 \pm 7$ and $\langle N_{part} \rangle > 71 \pm 7$ reproduced this dependence very well.

　　The significantly differing growth rates of $\langle \beta_T \rangle$ in regions $\langle N_{part} \rangle < 71 \pm 7$ ($\langle dN_{ch}/d\eta \rangle$ < 251 ± 20) and $\langle N_{part} \rangle > 71 \pm 7$ ($\langle dN_{ch}/d\eta \rangle$ > 251 ± 20) with T_0 staying constant within uncertainties in region $\langle N_{part} \rangle > 71 \pm 7$ ($\langle dN_{ch}/d\eta \rangle$ > 251 ± 20) probably indicate that $\langle N_{part} \rangle \approx 71 \pm 7$ ($\langle dN_{ch}/d\eta \rangle \approx 251 \pm 20$) is a threshold border value for a crossover transition from a dense hadronic state to the QGP phase (or mixed phase of QGP and hadrons) in Pb + Pb collisions at $\sqrt{s_{nn}}$ = 5.02 TeV. The threshold border value $\langle \beta_T \rangle \approx 0.46 \pm 0.03$ (corresponding to $\langle N_{part} \rangle \approx 71 \pm 7$ and $\langle dN_{ch}/d\eta \rangle \approx 251 \pm 20$), estimated in Pb + Pb collisions at $\sqrt{s_{nn}}$ = 5.02 TeV in the present analysis, agreed well with the corresponding border value $\langle \beta_T \rangle \approx 0.44 \pm 0.02$, recently obtained in Xe + Xe collisions at $\sqrt{s_{nn}}$ = 5.44 TeV in Ref. [24], and with almost constant $\langle \beta_T \rangle$ values extracted [20] in the BES program at the RHIC in central Au + Au collisions in $\sqrt{s_{nn}}$ = 7.7 − 39 GeV energy range, where the threshold for QGP production was reached [20,90–94].

　　The ratio (1.61 ± 0.24) of the estimated border values of $\langle N_{part} \rangle$ in Pb + Pb collisions at $\sqrt{s_{nn}}$ = 5.02 TeV and Xe + Xe collisions at $\sqrt{s_{nn}}$ = 5.44 TeV coincided with the ratio (1.59 ± 0.24) of the corresponding $\langle dN_{ch}/d\eta \rangle$ in these two collision types, and with the ratio of the mass

numbers of the corresponding ^{208}Pb and ^{132}Xe nuclei equal to $\frac{A(208_{Pb})}{A(132_{Xe})} \approx 1.58$. Hence, the relation $\frac{\langle N_{part} \rangle_{Pb+Pb}}{\langle N_{part} \rangle_{Xe+Xe}} \approx \frac{\langle dN_{ch}/d\eta \rangle_{Pb+Pb}}{\langle dN_{ch}/d\eta \rangle_{Xe+Xe}} \approx \frac{A(208_{Pb})}{A(132_{Xe})} \approx 1.6$ was satisfied.

The characters of T_0 versus $\langle \beta_T \rangle$ dependence were found to be considerably different in regions $\langle \beta_T \rangle < 0.46$ and $\langle \beta_T \rangle > 0.46$. The negative correlation between T_0 and $\langle \beta_T \rangle$ was quite strong in region $\langle \beta_T \rangle < 0.46$. In contrast to the strong negative correlation in region $\langle \beta_T \rangle < 0.46$, the correlation between parameters T_0 and $\langle \beta_T \rangle$ was significantly positive in region $\langle \beta_T \rangle > 0.46$. Hence, it was observed that not only does parameter $\langle \beta_T \rangle$ show significantly differing growth rates in regions $\langle N_{part} \rangle < 71 \pm 7$ ($\langle \frac{dN_{ch}}{d\eta} \rangle < 251 \pm 20$) and $\langle N_{part} \rangle > 71 \pm 7$ ($\langle \frac{dN_{ch}}{d\eta} \rangle > 251 \pm 20$), but also the character of correlation between parameters T_0 and $\langle \beta_T \rangle$ differs considerably in the corresponding intervals $\langle \beta_T \rangle < 0.46$ and $\langle \beta_T \rangle > 0.46$. This finding further supports our conjecture that $\langle N_{part} \rangle \approx 71 \pm 7$ ($\langle dN_{ch}/d\eta \rangle \approx 251 \pm 20$) is probably a threshold border value for a crossover transition from a dense hadronic state to the QGP phase (or mixed phase of QGP and hadrons) in Pb + Pb collisions at $\sqrt{s_{nn}} = 5.02$ TeV.

The non-extensivity parameter q demonstrates a systematic decrease with increasing $\langle N_{part} \rangle$ (collision centrality) for all studied particle species. This observation is in agreement with the known fact that the level of thermalization of the system increases with the increasing centrality of heavy-ion collisions at high energies. On the whole, the gap between q(mesons) and q(baryons) decreases with an increase in Pb + Pb collision centrality, and q(mesons) practically coincides within uncertainties with q(baryons) in central collisions with $\langle N_{part} \rangle > 160$. This could indicate quite a large degree of equilibrium and thermalization of QGP produced in central Pb + Pb collisions at $\sqrt{s_{nn}} = 5.02$ TeV with $\langle N_{part} \rangle > 160$.

References

1. Abelev, B. et al. [ALICE Collaboration] Centrality dependence of π, K, p production in Pb-Pb collisions at $\sqrt{s_{nn}}$ = 2.76 TeV. *Phys. Rev. C* **2013**, *88*, 044910. [CrossRef]
2. Abelev, B. et al. [ALICE Collaboration] Multiplicity Dependence of Pion, Kaon, Proton and Lambda Production in p-Pb Collisions at $\sqrt{s_{nn}}$ = 5.02 TeV. *Phys. Lett. B* **2014**, *728*, 25.
3. Aamodt, K. et al. [ALICE Collaboration] Strange particle production in proton-proton collisions at (s)$^{1/2}$ = 0.9 TeV with ALICE at the LHC. *Eur. Phys. J. C* **2011**, *71*, 1594. [CrossRef]
4. Adam, J. et al. [ALICE Collaboration] Multi-strange baryon production in p-Pb collisions at $\sqrt{s_{nn}}$ = 5.02 TeV. *Phys. Lett. B* **2016**, *758*, 389. [CrossRef]
5. Aamodt, K. et al. [ALICE Collaboration] Production of pions, kaons and protons in pp collisions at (s)$^{1/2}$ = 900 GeV with ALICE at the LHC. *Eur. Phys. J. C* **2011**, *71*, 1655. [CrossRef]

6. Adam, J. et al. [ALICE Collaboration] Production of K*(892)^0 and φ(1020) in p–Pb collisions at $\sqrt{s_{nn}}$ = 5.02 TeV. *Eur. Phys. J. C* **2016**, *76*, 245. [CrossRef]
7. Adam, J. et al. [ALICE Collaboration] K*(892)^0 and φ(1020) meson production at high transverse momentum in pp and Pb−Pb collisions at $\sqrt{s_{nn}}$ = 2.76 TeV. *Phys. Rev. C* **2017**, *95*, 064606. [CrossRef]
8. Adam, J. et al. [ALICE Collaboration] Enhanced production of multi-strange hadrons in high-multiplicity proton-proton collisions. *Nat. Phys.* **2017**, *13*, 535. [CrossRef]
9. Acharya, S. et al. [ALICE Collaboration] Multiplicity dependence of light-flavor hadron production in pp collisions at (s)$^{1/2}$ = 7 TeV. *Phys. Rev. C* **2019**, *99*, 024906. [CrossRef]
10. Acharya, S. et al. [ALICE Collaboration] Multiplicity dependence of (multi-)strange hadron production in proton-proton collisions at (s)$^{1/2}$ = 13 TeV. *Eur. Phys. J. C* **2020**, *80*, 167.
11. Acharya, S. et al. [ALICE Collaboration] Evidence of rescattering effect in Pb-Pb collisions at the LHC through production of K*(892)^0 and φ(1020) mesons. *Phys. Lett. B* **2020**, *802*, 135225.
12. Acharya, S. et al. [ALICE Collaboration] Production of pions, kaons, (anti-)protons and φ mesons in Xe–Xe collisions at $\sqrt{s_{nn}}$ = 5.44 TeV. *Eur. Phys. J. C* **2021**, *81*, 584. [CrossRef]
13. Khachatryan, V. et al. [CMS Collaboration] Strange particle production in pp collisions at (s)$^{1/2}$ = 0.9 and 7 TeV. *JHEP* **2011**, *5*, 064. [CrossRef]
14. Adair, A. et al. [CMS Collaboration] Study of the inclusive production of charged pions, kaons, and protons in pp collisions at (s)$^{1/2}$ =0.9, 2.76, and 7 TeV. *Eur. Phys. J. C* **2012**, *72*, 2164.
15. Chatrchyan, S. et al. [CMS Collaboration] Study of the production of charged pions, kaons, and protons in pPb collisions at $\sqrt{s_{nn}}$ = 5.02 TeV. *Eur. Phys. J. C* **2014**, *74*, 2847. [CrossRef]
16. Adler, C. et al. [STAR Collaboration] Multiplicity distribution and spectra of negatively charged hadrons in Au+Au collisions at $\sqrt{s_{nn}}$ = 130 GeV. *Phys. Rev. Lett.* **2001**, *87*, 112303.
17. Sirunyan, A.M. et al. [CMS Collaboration] Measurement of charged pion, kaon, and proton production in proton-proton collisions at (s)$^{1/2}$ = 13 TeV. *Phys. Rev. D* **2017**, *96*, 112003. [CrossRef]
18. Abelev, B.I. et al. [STAR Collaboration] Strange particle production in p+p collisions at (s)$^{1/2}$ = 200 GeV. *Phys. Rev. C* **2007**, *75*, 064901.
19. Adams, J. et al. [STAR Collaboration] Identified particle distributions in pp and Au+Au collisions at $\sqrt{s_{nn}}$ = 200 GeV. *Phys. Rev. Lett.* **2004**, *92*, 112301.
20. Adamczyk, L. et al. [STAR Collaboration] Bulk Properties of the Medium Produced in Relativistic Heavy-Ion Collisions from the Beam Energy Scan Program. *Phys. Rev. C* **2017**, *96*, 044904. [CrossRef]
21. Braun-Munzinger, P.; Koch, V.; Schäfer, T.; Stachel, J. Properties of hot and dense matter from relativistic heavy ion collisions. *Phys. Rept.* **2016**, *621*, 76. [CrossRef]
22. Burtebayev, N.; Fedosimova, A.; Lebedev, I.; Dmitriyeva, E.; Ibraimova, S.; Bondar, E.F. Fluctuations of Initial State and Event-by-Event Pseudo-Rapidity Correlations in High Energy Nuclear Collisions. *Universe* **2022**, *8*, 67. [CrossRef]
23. Olimov, K.K.; Liu, F.-H.; Musaev, K.A.; Shodmonov, M.Z. Multiplicity Dependencies of Midrapidity Transverse Momentum Distributions of Identified Charged Particles in proton-proton Collisions at (s)$^{1/2}$ = 7 TeV at the LHC. *Universe* **2022**, *8*, 174. [CrossRef]
24. Olimov, K.K.; Liu, F.-H.; Musaev, K.A.; Olimov, K.; Shodmonov, M.Z.; Fedosimova, A.I.; Lebedev, I.A.; Kanokova, S.Z.; Tukhtaev, B.J.; Yuldashev, B.S. Study of midrapidity pt distributions of identified charged particles in Xe+Xe collisions at (s$_{nn}$)$^{1/2}$ = 5.44 TeV using non-extensive Tsallis statistics with transverse flow. *Mod. Phys. Lett. A* **2022**, *37*, 2250095.
25. Aad, G. et al. [ATLAS Collaboration] Observation of a Centrality-Dependent Dijet Asymmetry in Lead-Lead Collisions at $\sqrt{s_{nn}}$ = 2.76 TeV with the ATLAS Detector at the LHC. *Phys. Rev. Lett.* **2010**, *105*, 252303.
26. Chatrchyan, S. et al. [CMS Collaboration] Jet momentum dependence of jet quenching in PbPb collisions at $\sqrt{s_{nn}}$ = 2.76 TeV. *Phys. Lett. B.* **2012**, *712*, 176.
27. Adamczyk, L. et al. [STAR Collaboration] Dijet imbalance measurements in Au + Au and pp collisions at $\sqrt{s_{nn}}$ = 200 GeV at STAR. *Phys. Rev. Lett.* **2017**, *119*, 062301. [CrossRef]
28. Adams, J. et al. [STAR Collaboration] Evidence from d + Au measurements for final state suppression of high p_T hadrons in Au+Au collisions at RHIC. *Phys. Rev. Lett.* **2003**, *91*, 072304.
29. Aamodt, K. et al. [ALICE Collaboration] Suppression of Charged Particle Production at Large Transverse Momentum in Central Pb + Pb Collisions at $\sqrt{s_{nn}}$ = 2.76 TeV. *Phys. Lett. B.* **2011**, *696*, 30. [CrossRef]
30. Chatrchyan, S. et al. [CMS Collaboration] Study of high-p$_T$ charged particle suppression in PbPb compared to pp collisions at $\sqrt{s_{nn}}$ = 2.76 TeV. *Eur. Phys. J. C.* **2012**, *72*, 1945.
31. Sirunyan, A.M. et al. [CMS Collaboration] Measurement of prompt and nonprompt charmonium suppression in PbPb collisions at 5.02 TeV. *Eur. Phys. J. C.* **2018**, *78*, 509. [PubMed]
32. Adamczyk, L. et al. [STAR Collaboration] Centrality and transverse momentum dependence of elliptic flow of multistrange hadrons and φ meson in Au+Au collisions at $\sqrt{s_{nn}}$ = 200 GeV. *Phys. Rev. Lett.* **2016**, *116*, 062301. [CrossRef]
33. Adare, A. et al. [PHENIX Collaboration] Scaling properties of azimuthal anisotropy in Au+Au and Cu+Cu collisions at $\sqrt{s_{nn}}$ = 200-GeV. *Phys. Rev. Lett.* **2007**, *98*, 162301.

34. Huovinen, P.; Kolb, P.; Heinz, U.W.; Ruuskanen, P.; Voloshin, S. Radial and elliptic flow at RHIC: Further predictions. *Phys. Lett. B* **2001**, *503*, 58. [CrossRef]

35. Acharya, S. et al. [ALICE Collaboration] Anisotropic flow of identified particles in Pb + Pb collisions at $\sqrt{s_{nn}}$ = 5.02 TeV. *JHEP* **2018**, *9*, 006.

36. Borsanyi, S.; Endrődi, G.; Fodor, Z.; Jakovác, A.; Katz, S.D.; Krieg, S.; Ratti, C.; Szabo, K.K. The QCD equation of state with dynamical quarks. *JHEP* **2010**, *2010*, 77.

37. Borsanyi, S.; Fodor, Z.; Hoelbling, C.; Katz, S.D.; Krieg, S.; Szabo, K.K. Full result for the QCD equation of state with 2 + 1 flavors. *Phys. Lett. B* **2014**, *730*, 99. [CrossRef]

38. Jiang, K.; Zhu, Y.; Liu, W.; Chen, H.; Li, C.; Ruan, L.; Tang, Z.; Xu, Z. Onset of radial flow in p+p collisions. *Phys. Rev. C* **2015**, *91*, 024910. [CrossRef]

39. Bashir, I.; Bhat, R.A.; Uddin, S. Evidence of collective flow in p-p collisions at LHC. *arXiv* **2015**, arXiv:1502.04185v2.

40. Bashir, I.; Parra, R.A.; Bhat, R.A.; Uddin, S. Particle Transverse Momentum Distributions in p-p Collisions at (s)$^{1/2}$=0.9 TeV. *Adv. High Energy Phys.* **2019**, *2019*, 8219567.

41. Khuntia, A.; Sharma, H.; Tiwari, S.K.; Sahoo, R.; Cleymans, J. Radial flow and differential freeze-out in proton-proton collisions at (s)$^{1/2}$=7 TeV at the LHC. *Eur. Phys. J. A* **2019**, *3*, 55.

42. Csanád, M.; Csörgő, T.; Jiang, Z.-F.; Yang, C.-B. Initial energy density of (s)$^{1/2}$ = 7 and 8 TeV p-p collisions at LHC. *Universe* **2017**, *3*, 9. [CrossRef]

43. Jiang, Z.F.; Csanad, M.; Kasza, G.; Yang, C.B.; Csorgo, T. Pseudorapidity and initial energy densities in p+p and heavy-ion collisions at RHIC and LHC. *Acta Phys. Pol. Proc. Suppl.* **2019**, *12*, 261. [CrossRef]

44. Tripathy, S.; Bisht, A.; Sahoo, R.; Khuntia, A.; Salvan, M.P. Event shape and multiplicity dependence of freeze-out scenario and system thermodynamics in proton + proton collisions at (s)$^{1/2}$ = 13 TeV using PYTHIA8. *Adv. High Energy Phys.* **2021**, *2021*, 8822524. [CrossRef]

45. Baker, O.K.; Kharzeev, D.E. Thermal radiation and entanglement in proton-proton collisions at energies available at the CERN Large Hadron Collider. *Phys. Rev. D* **2018**, *98*, 054007. [CrossRef]

46. Kharzeev, D.E.; Levin, E.M. Deep inelastic scattering as a probe of entanglement. *Phys. Rev. D* **2017**, *95*, 114008. [CrossRef]

47. Bergers, J.; Floerchinger, S.; Venugopalan, R. Dynamics of entanglement in expanding quantum fields. *JHEP* **2018**, *4*, 145. [CrossRef]

48. Bergers, J.; Floerchinger, S.; Venugopalan, R. Thermal excitation spectrum from entanglement in an expanding quantum string. *Phys. Lett. B* **2018**, *778*, 442. [CrossRef]

49. Olimov, K.K.; Liu, F.-H.; Musaev, K.A.; Olimov, K.; Tuktaev, B.J.; Yuldashev, B.S.; Saidkhanov, N.S.; Umarov, K.I.; Gulamov, K.G. Multiplicity dependencies of midrapidity transverse momentum spectra of identified charged particles in p+p collisions at (s)$^{1/2}$=13 TeV at LHC. *Int. J. Mod. Phys. A* **2021**, *36*, 2150149. [CrossRef]

50. Braun-Munzinger, P.; Redlich, K.; Stachel, J. Particle production in heavy ion collisions. In *Quark Gluon Plasma 3*; Hwa, R.C., Wang, X.-N., Eds.; World Scientific Publishing: Singapore, 2004.

51. Andronic, A.; Braun-Munzinger, P.; Stachel, J. Hadron production in central nucleus-nucleus collisions at chemical freezeout. *Nucl. Phys. A* **2006**, *772*, 167. [CrossRef]

52. Becattini, F.; Manninen, J.; Gazdzicki, M. Energy and system size dependence of chemical freeze-out in relativistic nuclear collisions. *Phys. Rev. C* **2006**, *73*, 044905. [CrossRef]

53. Andronic, A.; Braun-Munzinger, P.; Stachel, J. Thermal hadron production in relativistic nuclear collisions: The Hadron mass spectrum, the horn, and the QCD phase transition. *Phys. Lett. B* **2009**, *673*, 142. [CrossRef]

54. Stachel, J.; Andronic, A.; Braun-Munzinger, P.; Redlich, K. Confronting LHC data with the statistical hadronization model. *J. Phys. Conf. Ser.* **2014**, *509*, 012019. [CrossRef]

55. Zhang, Q.; Gao, Y.-Q.; Liu, F.-H.; Olimov, K.K. An Energy Independent Scaling of Transverse Momentum Spectra of Direct (Prompt) Photons from Two-Body Processes in High-Energy Proton–Proton Collisions. *Ann. Phys.* **2022**, *534*, 2100567. [CrossRef]

56. Schnedermann, E.; Sollfrank, J.; Heinz, U. Thermal phenomenology of hadrons from 200 A GeV S+S collisions. *Phys. Rev. C* **1993**, *48*, 2462. [CrossRef] [PubMed]

57. Acharya, S. et al. [ALICE Collaboration] Production of charged pions, kaons and (anti-)protons in Pb-Pb and inelastic pp collisions at $\sqrt{s_{nn}}$ = 5.02 TeV. *Phys. Rev. C* **2020**, *101*, 044907.

58. Abelev, B.I. et al. [STAR Collaboration] Systematic measurements of identified particle spectra in pp, d+Au, and Au+Au collisions at the STAR detector. *Phys. Rev. C* **2009**, *79*, 034909. [CrossRef]

59. Abelev, B.I. et al. [STAR Collaboration] Identified particle production, azimuthal anisotropy, and interferometry measurements in Au+Au collisions at $\sqrt{s_{nn}}$ = 9.2 GeV. *Phys. Rev. C* **2010**, *81*, 024911.

60. Tang, Z.B.; Xu, Y.; Ruan, L.; van Buren, G.; Wang, F.; Xu, Z. Spectra and radial flow in relativistic heavy ion collisions with Tsallis statistics in a blast-wave description. *Phys. Rev. C* **2009**, *79*, 051901. [CrossRef]

61. Lao, H.L.; Lao, H.-L.; Liu, F.-H.; Lacey, R.A. Extracting kinetic freeze-out temperature and radial flow velocity from an improved Tsallis distribution. *Eur. Phys. J. A* **2017**, *53*, 44. [CrossRef]

62. Khandai, P.K.; Sett, P.; Shukla, P.; Singh, V. System size dependence of hadron pT spectra in p+p and Au+Au collisions at $\sqrt{s_{nn}}$ = 200 GeV. *J. Phys. G* **2014**, *41*, 025105. [CrossRef]

63. Olimov, K.K.; Kanokova, S.Z.; Olimov, A.K.; Umarov, K.I.; Tukhtaev, B.J.; Gulamov, K.G.; Yuldashev, B.S.; Lutpullaev, S.L.; Saidkhanov, N.S.; Olimov, K.; et al. Combined analysis of midrapidity transverse momentum spectra of the charged pions and kaons, protons and antiprotons in p+p and Pb + Pb collisions at $(s_{nn})^{1/2}$ = 2.76 and 5.02 TeV at the LHC. *Mod. Phys. Lett. A* **2020**, *35*, 2050237. [CrossRef]
64. Olimov, K.K.; Kanokova, S.Z.; Olimov, K.; Gulamov, K.G.; Yuldashev, B.S.; Lutpullaev, S.L.; Umarov, F.Y. Average transverse expansion velocities and global freeze-out temperatures in central Cu+Cu, Au+Au, and Pb + Pb collisions at high energies at RHIC and LHC. *Mod. Phys. Lett. A* **2020**, *35*, 2050115.
65. Zhang, X.; Liu, F.; Olimov, K.K. A systematic analysis of transverse momentum spectra of J/ψ mesons in high energy collisions. *Int. J. Mod. Phys. E* **2021**, *30*, 2150051. [CrossRef]
66. Li, L.; Liu, F.; Olimov, K.K. Excitation Functions of Tsallis-Like Parameters in High-Energy Nucleus–Nucleus Collisions. *Entropy* **2021**, *23*, 478. [CrossRef]
67. Wang, Q.; Liu, F.; Olimov, K.K. Initial-State Temperature of Light Meson Emission Source From Squared Momentum Transfer Spectra in High-Energy Collisions. *Front. Phys.* **2021**, *9*, 792039. [CrossRef]
68. Karsch, F.; Laermann, E. Thermodynamics and in-medium hadron properties from lattice QCD. In *Quark-Gluon Plasma 3*; Hwa, R.C., Wang, X.-N., Eds.; World Scientific: Singapore, 2004.
69. Bazavov, A. et al. [HotQCD Collaboration] The chiral and deconfinement aspects of the QCD transition. *Phys. Rev. D* **2012**, *85*, 054503. [CrossRef]
70. Busza, W.; Rajagopal, K.; Van der Schee, W. Heavy Ion Collisions: The Big Picture, and the Big Questions. *Ann. Rev. Nucl. Part. Sci.* **2018**, *68*, 339. [CrossRef]
71. Tsallis, C. Enthusiasm and Skepticism: Two Pillars of Science—A Nonextensive Statistics Case. *Physics* **2022**, *4*, 609. [CrossRef]
72. Rocha, L.Q.; Megías, E.; Trevisan, L.A.; Olimov, K.K.; Liu, F.; Deppman, A. Nonextensive Statistics in High Energy Collisions. *Physics* **2022**, *4*, 659–671. [CrossRef]
73. Tsallis, C. Possible generalization of Boltzmann-Gibbs statistics. *J. Statist. Phys.* **1988**, *52*, 479. [CrossRef]
74. Tsallis, C. Nonadditive entropy: The concept and its use. *Eur. Phys. J. A* **2009**, *40*, 257. [CrossRef]
75. Cleymans, J.; Worku, D. The Tsallis distribution in proton–proton collisions at (s)1/2 = 0.9 TeV at the LHC. *J. Phys. G* **2012**, *39*, 025006.
76. Sena, I.; Deppman, A. Systematic analysis of p_T -distributions in p+p collisions. *Eur. Phys. J. A* **2013**, *49*, 17. [CrossRef]
77. Adare, A. et al. [PHENIX Collaboration] Measurement of neutral mesons in p+p collisions at $(s)^{1/2}$ = 200 GeV and scaling properties of hadron production. *Phys. Rev. D* **2011**, *83*, 052004.
78. Khandai, P.K.; Sett, P.; Shukla, P.; Singh, V. Hadron spectra in p+p collisions at RHIC and LHC energies. *Int. J. Mod. Phys. A* **2013**, *28*, 1350066. [CrossRef]
79. Wong, C.Y.; Wilk, G. Tsallis Fits to p_T Spectra for pp Collisions at LHC. *Acta Phys. Polon. B* **2012**, *43*, 2047. [CrossRef]
80. Cleymans, J.; Lykasov, G.I.; Parvan, A.S.; Sorin, A.S.; Teryaev, O.V.; Worku, D. Systematic properties of the Tsallis Distribution: Energy Dependence of Parameters in High-Energy p-p Collisions. *Phys. Lett. B* **2013**, *723*, 351. [CrossRef]
81. Cleymans, J. On the Use of the Tsallis Distribution at LHC Energies. *J. Phys. Conf. Ser.* **2017**, *779*, 012079. [CrossRef]
82. Zheng, H.; Zhu, L. Comparing the Tsallis Distribution with and without Thermodynamical Description in p-p Collisions. *Adv. High Energy Phys.* **2016**, *2016*, 9632126. [CrossRef]
83. Bíró, G.; Barnaföldi, G.G.; Biró, T.S.; Ürmössy, K.; Takács, Á. Systematic Analysis of the Non-Extensive Statistical Approach in High Energy Particle Collisions—Experiment vs. *Theory. Entropy* **2017**, *19*, 88. [CrossRef]
84. Wilk, G.; Wlodarczyk, Z. Interpretation of the Nonextensivity Parameter q in Some Applications of Tsallis Statistics and Lévy Distributions. *Phys. Rev. Lett.* **2000**, *84*, 2770. [CrossRef] [PubMed]
85. Olimov, K.K.; Iqbal, A.; Masood, S. Systematic analysis of midrapidity transverse momentum spectra of identified charged particles in p + p collisions at $(s)^{1/2}$ = 2.76, 5.02, and 7 TeV at the LHC. *Int. J. Mod. Phys. A* **2020**, *35*, 2050167.
86. Aamodt, K. et al. [ALICE Collaboration] The ALICE experiment at the CERN LHC. *JINST* **2008**, *3*, S08002. [CrossRef]
87. Acharya, S. et al. [ALICE Collaboration] Centrality Determination in Heavy Ion Collisions. CERN Report ALICE-PUBLIC-2018-011. Available online: https://cds.cern.ch/record/2636623 (accessed on 1 June 2022).
88. Tsallis, C.; Mendes, R.S.; Plastino, A.R. The role of constraints within generalized nonextensive statistics. *Phys. A* **1998**, *261*, 534. [CrossRef]
89. Biro, T.S.; Purcsel, G.; Ürmössy, K. Non-extensive approach to quark matter. *Eur. Phys. J. A* **2009**, *40*, 325. [CrossRef]
90. Afanasiev, S. et al. [NA49 Collaboration] Energy dependence of pion and kaon production in central Pb + Pb collisions. *Phys. Rev. C* **2002**, *66*, 054902.
91. Anticic, T. et al. [NA49 Collaboration] Energy and centrality dependence of deuteron and proton production in Pb + Pb collisions at relativistic energies. *Phys. Rev. C* **2004**, *69*, 024902.
92. Alt, C. et al. [NA49 Collaboration] Energy and centrality dependence of ‾p and p production and the Λ/‾p ratio in Pb + Pb collisions between 20 A GeV and 158 A GeV. *Phys. Rev. C* **2006**, *73*, 044910. [CrossRef]
93. Alt, C. et al. [NA49 Collaboration] Pion and kaon production in central Pb + Pb collisions at 20 A and 30 A GeV: Evidence for the onset of deconfinement. *Phys. Rev. C* **2008**, *77*, 024903. [CrossRef]
94. Cleymans, J.; Oeschler, H.; Redlich, K.; Wheaton, S. The thermal model and the transition from baryonic to mesonic freeze-out. *Eur. Phys. J. A* **2006**, *29*, 119. [CrossRef]

95. Biro, G.; Barnaföldi, G.G.; Biro, T.S.; Shen, K. Mass hierarchy and energy scaling of the Tsallis—Pareto parameters in hadron productions at RHIC and LHC energies. *EPJ Web Conf.* **2018**, *171*, 14008. [CrossRef]

96. Tawfik, A.N.; Yassin, H.; Elyazeed, E.R.A. Particle Yields and Ratios within Equilibrium and Non-Equilibrium Statistics. *Europhys. Lett.* **2019**, *126*, 41001. [CrossRef]

97. Yassin, H.; Elyazeed, E.R.A.; Tawfik, A.N. Transverse momentum spectra of strange hadrons within extensive and nonextensive statistics. *Phys. Scr.* **2020**, *95*, 075305. [CrossRef]

98. Tawfik, A.N.; Yassin, H.; Yassin, H.; Yassin, H. Extensive/nonextensive statistics for p_T distributions of various charged particles produced in p + p and A + A collisions in a wide range of energies. *arXiv* **2019**, arXiv:1905.12756v2.